2012-01-01

DNA-Carbon Nanotubes Composites As Gene Sensors

Hugo Alarcon
University of Texas at El Paso, hvalarcon@miners.utep.edu

DNA-CARBON NANOTUBES COMPOSITES AS GENE SENSORS

HUGO ALARCON VALENZUELA

Department of Chemistry

Approved:

_____
Juan C. Noveron, Ph.D., Chair

_____
Russell Chianelli, Ph.D

_____
German Rosas-Acosta, Ph. D

_____
Ricardo Bernal, Ph. D

_____
Benjamin C. Flores, Ph.D.
Dean of Graduate School

DEDICATION

I am very grateful to my family and fiancé for all of their support throughout my stay in the master's program. I want to thank my mother and father for their overwhelming love and support when I needed it the most, I love you guys very much. I would also like to like to thank my brother for his words of encouragement when I needed them the most. Finally, I am very grateful to my girlfriend for all the support and comprehension throughout the last few years.

DNA-CARBON NANOTUBES COMPOSITES AS GENE SENSORS

by

HUGO ALARCON VALENZUELA, MICROBIOLOGY B.S

THESIS

Presented to the Faculty of Graduate School of

The University of Texas at El Paso

in partial fulfillment

of the requirements

for the degree of

MASTER OF SCIENCE

Department of Chemistry

THE UNIVERSITY OF TEXAS AT EL PASO

December 2012

ACKNOWLEDGMENTS

This research was carried out as part of the carbon nanotube gene sensor project headed by Dr. Juan C. Noveron. I am tremendously grateful for the unique opportunity of having been a part of so many of Dr. Noveron's challenging projects. Also I am deeply thankful for your support as a friend when things got difficult.

I would like to acknowledge all of the people that helped me in this project either by aiding with analysis, providing chemicals or just provided friendly advice; Mariam Viveros, Ted Whitworth, Enrique Ramirez, Neti Venkata, Emmanuel Zubia, Parijat, and Ricardo McCreary. Especial thanks to Dr. Xiao's group for the use of the light scattering device, and of course I would like to thank all the people in my lab, thank you guys.

Without the financial support of the Border Biomedical Research Center this project would not have come to realization, so thank you very much. I would also like to acknowledge the Chemistry department and its entire faculty for their advice and help. All research in this thesis was conducted in Dr. Noveron's laboratory at the University of Texas at El Paso.

ABSTRACT

Carbon fullerenes are unusually structured molecules with robust mechanical and electronic properties. Their versatility is astounding; envisioned applications range from field emission displays to impregnated metal composites, battery storage media, and nanoelectronic devices. The combination of simple constituency, diverse behavior, and ease of fabrication makes these materials a cornerstone topic in current research.

This work describes experiments conducted on nanotubes using Dynamic light scattering (DLS). The aim is to detect cluster formation from individual carbon nanotube (CNT) solutions using a nanotube DNA binding sequence and a secondary recognizing complementary DNA sequence to bind neighboring CNTs. Dynamic Light Scattering is an available method for characterization of particles in solution and size determination of them based on their dynamics in solution. The size detection window of this technique makes it uniquely suited for observing sequence specific CNT aggregation.

Although both functionalized Multi-Wall carbon nantoubes (f-MWCNTs) and functionalized single-wall carbon nanotubes (f-SWNTs) were explored in this thesis the primary subject of this study is a glycosylated Single-Wall carbon nanotube (SWCNT-Glycol).

Measurements indicate that the most adept type of CNT for aggregation studies is the SWCNT-Glycol, with superior dispersibility and smaller aggregates that fall within detection limit. In particular it did demonstrate to aggregate only when the binding DNA sequences were introduced into the sample.

TABLE OF CONTENTS

LIST OF FIGURES

LIST OF FIGURES

CHAPTER 1

1.1 Overview

Carbon nanotubes belong to a family of molecules known as Fullerenes along with Buckyballs and ellipsoid shaped carbon molecules. These materials possess robust mechanical and electronic properties. Their versatility is incredible; proposed applications range from gene sensors, emission displays, material enforcer, battery storage media, nanoelectronic devices, and thermal therapy. The fact that these molecules have so many interesting properties makes them a cornerstone topic in current research.

Carbon nanotubes research is currently advancing at a very fast pace since the keen observations of Dr. Ijima, ever since there has been an enormous number of publications in the subject. According to the Science Direct web of knowledge database for articles with the search criteria "carbon nanotube" yields over 50,000 references. Analyzing these references by publication year, we can see that there is an exponential growth in number with time as is shown in Figure 1.

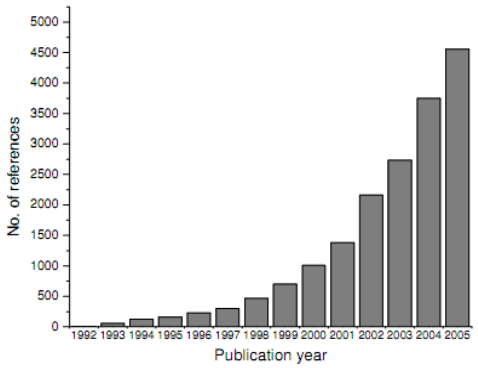

Figure 1. Graph showing the increase in CNT references in thirteen years

This thesis details the functionalization and characterization of CNTs, as well as our attempt to use them as a platform for universal gene sensors. Our design is based on the fact that CNTs are known to interact with DNA making them an ideal target for binding genes that then can be recognized by complementary sequences causing pronounced CNT aggregation. To provide a cost effective method for gene sensing we proposed using Dynamic Light Scattering (DLS) to detect the sequence specific size change of positive gene detection.

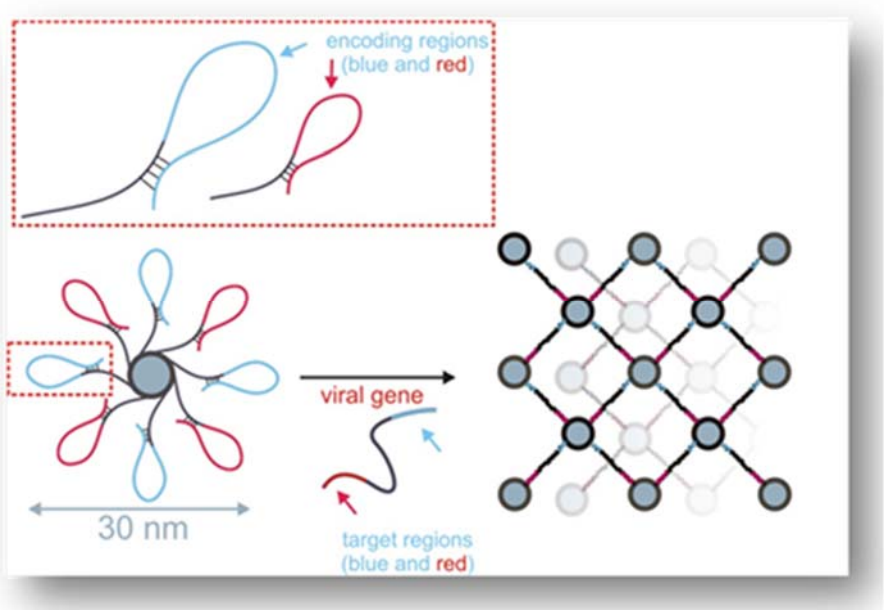

Illustration 1. Sketch depicting the sequence dependent aggregation of CNTs

In order to convert a CNT into a gene sensor, we carried out a systematic study of plain and functionalized CNTs interactions with DNA strands and analyze how size and chemical composition such as multiwall carbon nanotubes (MWCNTs) and single wall carbon nanotubes (SWCNTs) improved the solubility and suitable properties conducive to our design. Finally to distinguish between the natural tendency of CNTs to aggregate and gene specific CNT agglomeration we explored incubation times, and other parameters to optimize the system. The body of this work is arranged as follows: Chapter 1 introduces the background material essential for the following chapters. Chapter 2 details the instrumentation, materials and procedures.

Chapter 4 presents the results and their analysis. Finally, Chapter 5 gives a short summary of the findings.

1.2 Background

This section is essential for the interpretation of the results presented in subsequent chapters. A brief description on the some carbon allotropes, the history, properties, synthesis, applications and characterization of CNTs is provided, followed by an introduction to Dynamic Light Scattering.

1.2.1 Carbon allotropes

Carbon is a very versatile element, so much that it can form a myriad of compounds with other elements to give thousands of new chemicals with exciting properties. Though carbon does not only have the capability of bonding with other elements, but does so with itself in different ways forming what are known as allotropes. These allotropic materials may differ in the lattice structure that they form as crystals, the type of hybridization of each carbon, or a conjunction of both. There are many different carbon allotropes with very different physical properties; in fact we still keep on discovering new forms like the carbon nanofoam. Nonetheless in this section I will give a quick overview on seven of the known carbon allotropes; elemental carbon, graphite, amorphous carbon, lonsdaleite, glassy carbon, diamond, and fullerenes.

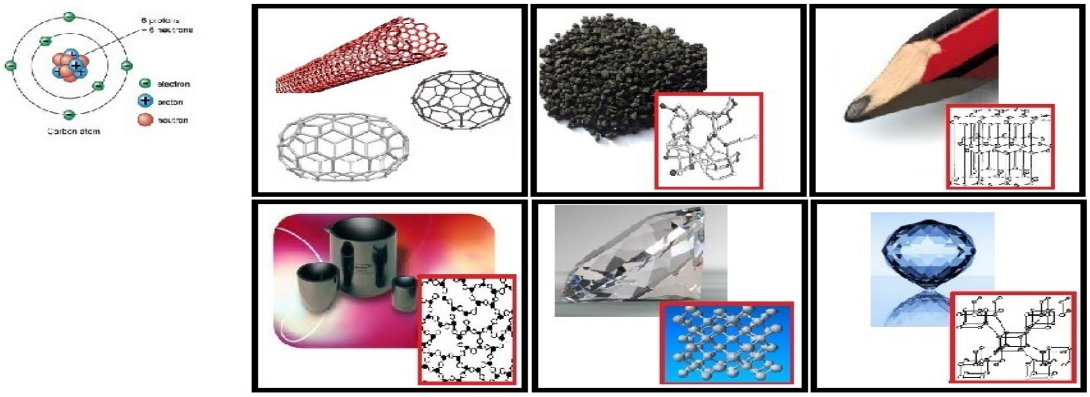

Figure 2. Known allotropes of carbon with atomic arrangement. First row from left to right; atomic carbon, fullerenes, amorphous carbon and graphite. Second row; glassy carbon, diamond, and lonsdaleite

1.2.2 Elemental carbon

The carbon element is present in every living organism in the planet, also our civilization has taken advantage of chemical manipulation to incorporate organic molecules even into our furniture. Mainly, the reason why carbon presence is so widespread is because of the stability and versatility of the atom. The carbon element is number six in the periodic table and it contains four valence electrons only two of which are present in the p-subshell. The unique electronic configuration allows it to form different molecular geometries (Fig 3). Of the various forms of solid carbon, the two most abundant allotropes are diamond and graphite (Fig.2).

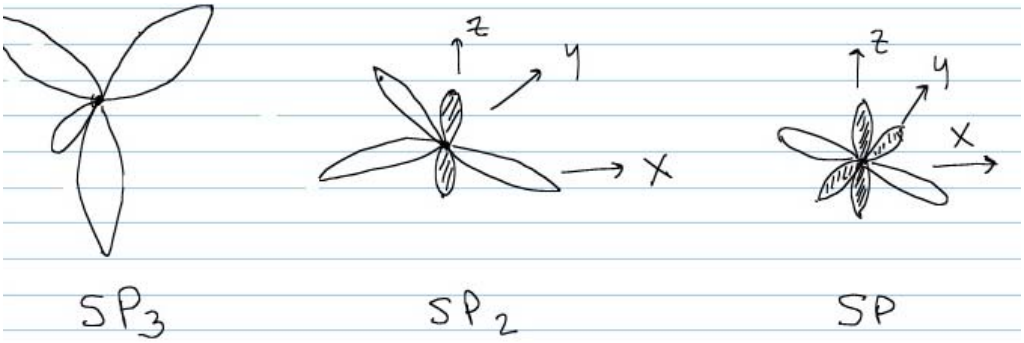

Illustration 2. Drawing depicting the hybridization states of carbon. Shaded lobes represent free p-orbitals and the remaining lobes are used to bond with other orbitals.

1.2.3 Diamond

One of the many allotropes of carbon is the highly valued diamond. Throughout history the material has been of been of great value and accessible only to those of great wealth, thought chemically is not the most stable of the allotropes. The precious diamond material is solely composedofsp3 hybridized carbon atoms that disperse in three dimensions to form one of the toughest materials know today (Fig.1). It is known for its extraordinary hardness, and its insulating properties with a known band gap of 5.5 eV. Under normal standard temperature and pressure conditions the material is only metastable, but a large activation energy barrier retards its decay rate into the more stable graphite state to geologic time scales.

1.2.4 Graphite

Graphite is composed of stacked sheets of sp2 carbons with a hexagonal lattice structure, (Figure 2). The inter-planar carbon sheets are held together by very weak pi-pi stacking interaction allowing easy gliding of the sheets, making graphite a good lubricant in the automotive industry. This inter-planar orbital pi-interaction gives the material semi metallic conduction properties.

1.2.5 Amorphous carbon

This form of carbon doesn't have an ordered structure, and thus its name (Figure 2). This material due to its large surface area and porosity has been used for chemical removal. It is easily produced through the pyrolysis of carbon containing materials like coal or soot, under normal conditions. Because of its abundance and easy access is a cheap alternative it has been used for the remediation of contaminated sites in the different ecosystems (19).

1.1.5 Lonsdaleite

Lonsdaleite is thought to form from graphite precursors in meteorites upon impact with earth. It has also been synthesized from the polyhydrocarbyne (20). It is a material very similar to diamond with a hexagonal crystal lattice (Figure 2.)

1.1.6 Glassy Carbon

Yet another allotrope of carbon, glassy carbon, was fabricated in England by Dr. Redfern in fifties in an attempt to find a material that would mirror diamond (Figure 2). The glass-like material was prepared using a phenolic resin without the use of a catalyst, but subjected to very high temperatures. This allotrope is very chemically inert including resistance to oxidation by acids even after several months of treatment. It has been utilized as electrode material in electrochemistry (18).

Glassy carbon is also known as vitreous carbon and is composed of randomly oriented micro fibrils 15-50 A wide (17), that twist and bend to form pronounced inter-fibrillar nodes. It has a very low density (1.4-1.5 g/cm^3), compared to diamond (3.52 g/cm^3), and graphite (2.27 g/cm^3), (17).

1.1.7 Fullerenes

1.1.7.1 Buckyballs

Another allotrope of carbon is the fullerene family, which include carbon nanotubes and Buckyballs. Even though scientists had proposed the possibility of close caged carbon molecules until the seventies (2), the presence of fullerenes wasn't proven until fifteen years later (3). Researchers had accomplished through laser ablation of graphite the formation of carbon clusters that turned to be 10-30 atom rings and 60 and 70 member molecules(4). Scientist very soon theorized that the bigger molecules were of closed cage configuration. The term "fullerene" was introduced in recognition of R. Buckminster Fuller, a renowned architect for his geodesic dome constructions.

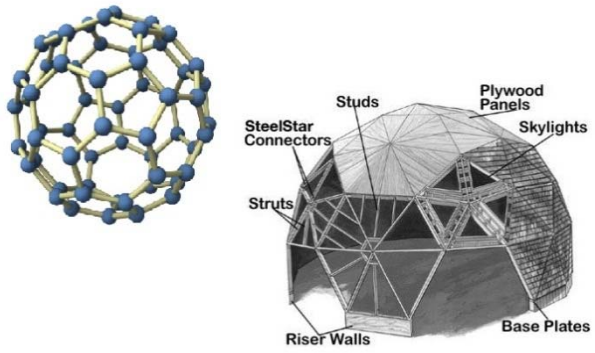

Figure 3. Comparison of a Buckyball fullerene (left) and R. Buckminster Fuller geodesic dome (right). Note the similitude of the structures

The Buckyball lattice structure is similar to the hexagonal graphite lattice in that it consists of a 2-dimensionalsurface. In order to achieve the curvature needed to achieve the cage structure, the replacement of some hexagons for pentagons is required. To be more exact Euler's

theory dictated that twelve faces have to be pentagonal. Therefore the smallest possible fullerene (C_{20}) is composed onlyof12pentagons. Still the cage curvature made also introduces a lot of strain energy in the molecule making small Buckyballs very unstable. This source of instability is minimized by separating the pentagon faces as much as possible, though the smallest buckyball without adjacent pentagon faces is C_{60}. The molecular stability of C_{60} is reflected by it abundance in any buckyball growth process, typically six times more abundant than the next more abundant product, C_{70}.

The C_{60} buckyball is composed of 20 hexagonal and 12 pentagonal faces in a spherical arrangement. The carbon bonds that constitute the rich sp^2 system can be either single bonds along the 60 pentagonal edges, with 1.46 Å in length, and 30 double bonds between the neighboring hexagons, which are1.40 Å in length (5). Studies with NMR have shown that the average molecular diameter is only 7.10Å (6).

1.1.7.2 Carbon Nanotubes

Carbon nanotube type fullerenes were discovered by Japanese researcher Ijima in 1991 (1), these diverse potential applications have captivated researchers. In spite of having a simple chemical constitution, nanotubes demonstrate an astounding mix of physical properties, like chemical resistance, large aspect ratios, and amazing field emission properties. Of particular technological importance is that based on the orientation of the carbon bonds in the molecular layout, they can be metallic or semiconducting materials, which makes them a natural target for the development of nanoelectronics.

Although C_{60} has very good structural stability, larger structure can be constructed by the propagation of benzene rings along the diameter of the buckyball to form tube-like structures. Ideally, nanotubes are flawless cylinders composed ofsp^2 carbons in an hexagonal lattice and

capped at either end by a half buckyball. Because of its striking atomic layout one can easily picture these structures being formed by rolling a graphene sheet onto itself and close into a tube. (Figure 5).These carbon allotropes are unique in shape, size, and possess outstanding chemical behavior.

Due to their many qualities carbon nanotube have potential applications in the biological nanotechnology emerging field. Nonetheless, the actual uses have been greatly limited due to their reduced solubility in water. An alternative to dissolve or disperse these materials is by surface modification with water soluble side moieties, such as carboxyl group (7), polyethylene glycol (8-10), amino groups (11), hydroxyl group (12), and many others (13-15).Just as well in order to increase their biocompatibility they have been functionalized with biocompatible molecules like the abundant membrane molecule phosphoryl choline (16).

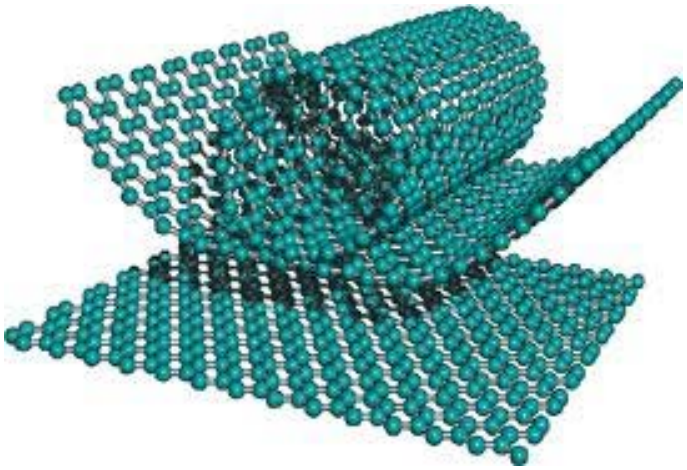

Figure 4. Model to represent the similitudes between the two graphite sheets on the bottom and the single wall CNT, (adapted from ref.12).

1.2 Carbon nanotubes background

Nanotubes are classified in two categories derived from their diameter size. If is the diameter is on the order of one nanometer, while a couple of microns in length, they are categorized as single-walled nanotubes (SWNTs). On the other hand if the tube is composed of several concentrical tubes reaching an overall diameter of a few nanometers they are to be called

multi-walled nanotubes (MWNTs). Multi-wall nanotubes may consist of one up to tenths and hundreds of concentric shells of carbons with adjacent wall separation of 0.34 nm. Furthermore these can be further categorized into semi-conducting or metallic depending on their structural parameters.

1.2.1Single-wall carbon nanotubes

These types of tubes are usually a made in smaller proportions in the common synthetic techniques, therefore more difficult to purify as well. The often mentioned superb properties generally refer to SWNTs. As previously mentioned, they are graphite like tubes that have at least one side capped by a half Buckyball. The caps are made by the addition of some pentagons, and so these caps are the main reason that nanotubes are considered relatives of buckminsterfullerene (buckyball) a roughly spherical molecule made of sixty carbon atoms, that looks like a soccer ball

The observed diameters for these structures are between one to two nanometers, although the diameter depends on the conditions used to synthesize them. SWNTs are more pliable than their multi-walled counterparts and can be twisted, flattened and bent into small circles or around sharp bends without breaking.

The majority of SWNTs have a 1 nm diameter, with a length that can go from a couple hundred nanometers to a couple of microns. These types of tubes exhibit interesting electric properties that are not shared by their multi-walled carbon nanotubes (MWNT) relatives.

1.2.1.1 Molecular structure

Just like in graphite each sp2 carbon in the CNT layout is held together by three neighbor atoms. There are three possible final conformations in which the sp^2 carbon can arrange themselves, giving them different physical properties.

Just like as introduced in any Organic Chemistry course, the terms *Armchair* and *Zig-Zag* refer to the arrangement of the carbons in a cyclohexane molecule; structures arising to alleviate some strain energy. In order to deal with some of the atomic crowding that comes with such large structures carbon atoms come out of plane and rearrange in more stable conformations. Using the unit cell of the CNT and drawing a vector describing the atomic dimensions only three orientations have been spotted so far. The (m, n) vectors nine and zero correspond to the zigzag orientation, the squared unit cell coming from (5, 5) comes from the armchair orientation, and finally and mixture comes from the (9, 5) vectors named the chiral structure.

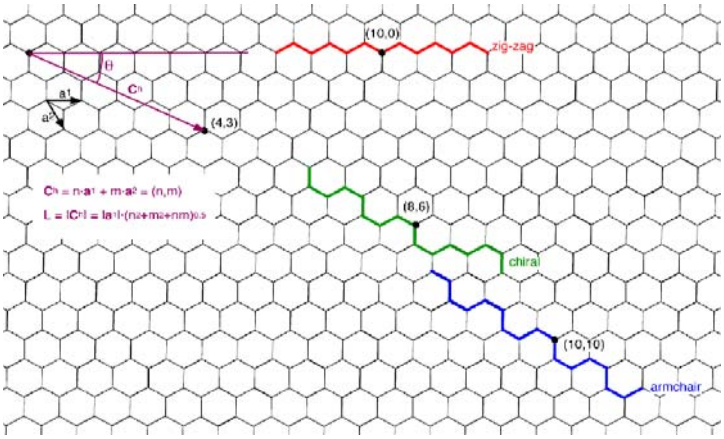

Figure 5. De Heer abacus used to explain (m, n) vectors that determine the final orientation of each tube. An (n, m) tube, move n times a1 and m times a2 from the origin to get to point (n, m) and roll-up the sheet so that the two points coincide.

Basically, one can roll up the tube along one of the symmetry axis: this gives either an armchair tube or a zig-zag tub. It is also possible to roll up the sheet in a direction that differs from a symmetry axis: one obtains a chiral nanotube, in which the equivalent atoms of each unit cell are aligned on a spiral. Besides the chiral angle, the circumference of the cylinder can also be varied. In general, the whole family of nanotubes is classified as zigzag, armchair, and chiral tubes of different diameters:

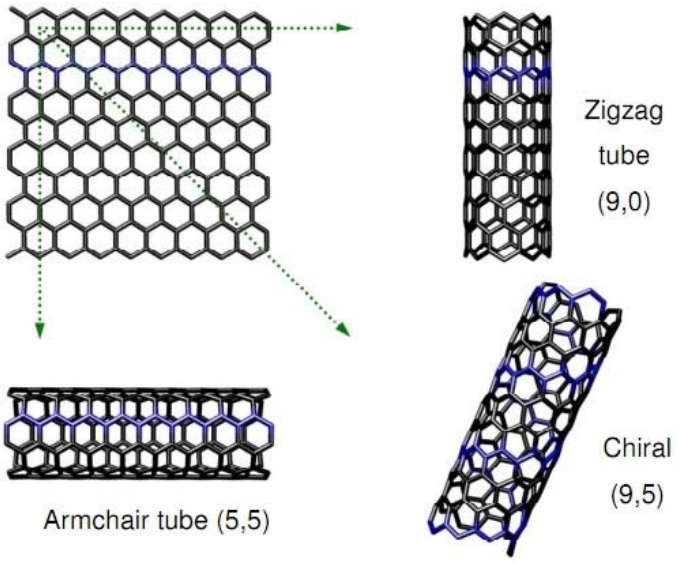

Figure 6. Potential carbon-carbon bond orientations on CNTs can change their physical properties dramatically.

1.2.2 Multi-wall carbon nanotubes

Multi-walled nanotubes (MWNT) consist of multiple rolled in on themselves to form a tube shape. Sheets of graphite are arranged in concentric cylinders with potentially several layers. The interlayer distance in multi-walled nanotubes is close to the distance between graphene layers in graphite, approximately 0.33 nm.

Although synthetic procedures have higher yields for MWNTs than SWNTs, their structures are less well understood than single-wall nanotubes because of their greater complexity and variety. Many of the nanotube applications now being considered or put into practice involve multi-walled nanotubes, because they are easier to produce in large quantities at a reasonable price and have been available in decent amounts for much longer than SWNTs.

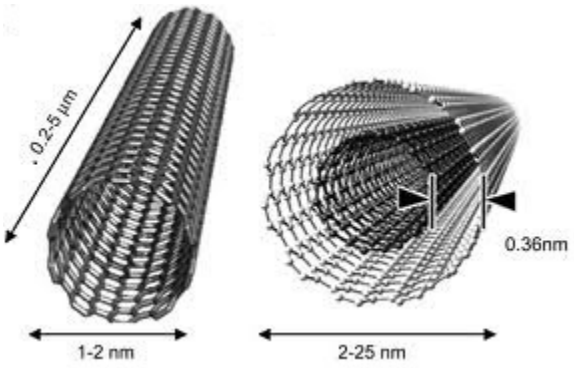

Figure 7. Model of the size difference in both length and diameter of SWCNT, on the left, and MWCNT, on the right.

Chemical bonding on a nanotubes is explained by physical chemistry more specifically the orbital hybridization resulting from the structure. The layout of the molecule is uniquely constructed of sp^2 hybridized carbon bonds, similar to those of graphite. This type of bonding is stronger than the sp^3 bonds found in diamond, provides this material its unique strength. CNTs interact with each other, through van der wall forces, entangling each other, just like ropes making a not.

1.2.3 Carbon nanotube physical properties

Several studies have shown that CNTs have many interesting physical properties. The aromatic tubes have shown to be as better conductors as copper but can carry as much as 4 $x10^9$ A/cm^3, making them three orders of magnitude higher than copper or aluminum in current carrying capacity (22). They also possess high carrier mobility reaching 10,000 cm^2/Vs. Not only they have astounding electrical properties, but they have shown to also been one of the stiffest and strongest materials known to man with a Young's modulus of over 1 Terapascal being just as stiff as diamond, and a tensile strength of 200 gigapascal (23). They have also demonstrated to be excellent thermal conductors with an astounding 3000 W/mK, conductivity better than all but the purest diamond, excellent materials for thermal management (24).

1.2.3.1 Mechanical properties

Carbon nanotubes are the stiffest and strongest material known to man today, in terms of

its outstanding elastic modulus and tensile strength respectively. This strength results from the covalent sp^2 bonds formed between individual carbon atoms. The carbon atoms of a single sheet of graphite form a planar honeycomb lattice are connected via strong chemical bonds to three neighboring carbon atoms. Carbon nanotubes are stiffer than steel, and are very resistant to damage from physical and chemical forces. Not only is a very strong material, but also pressing the tip of a nanotube will only cause it to bend, but without breakage or deformation after force seizes. This property makes CNTs very useful as probe tips for very high-resolution scanning probe microscopy. Quantifying these effects has been rather difficult, and an exact numerical value has not been agreed upon (30)

The current Young's modulus value of single walled nanotubes is about 1 TeraPascal, though this data has been argued greatly, and measurements as 1.8 Tpa have been reported. These differences probably arise through different experimental measurement techniques. Others have shown theoretically that the Young's modulus depends on the size and chirality of the single walled nanotubes, ranging from 1.22 Tpa to 1.26 Tpa (30). However, when dealing with MWCNT the modulus measurements don't strongly depend on the diameter, but correlates to the amount of disorder in the nanotube walls. To be expected the outermost layers break first in multi-wall nanotubes.

Nanotubes though are not that resistant to compression, because of their hollow structure and high aspect ratio, they tend to undergo buckling when placed under compressive forces.

1.2.3.2 Thermal properties

Carbon nanotubes are very good thermal conductors dispersing heat efficiently thou ought the tube, but are good insulators laterally to the tube axis (31). The temperature stability of CNTs is established to be up to 2800^{o}C in vacuum or 750^{o}Cin air. Preliminary experiments and

simulation studies on the thermal properties of CNTs show very high thermal conductivity. It is expected, therefore, that nanotube reinforcements in polymeric materials may also significantly improve the thermal and thermo mechanical properties of the composites.

1.2.3.4 High-aspect ratio Properties

Though nanotubes are very small materials they have very high aspect ratio conductive additive for plastics of all types. Their high aspect ratio means that these materials have very large loading capacity and therefore are ideal materials molecular carriers. Through pi-pi stacking interactions these molecules can load and maintain lots of molecules adhered to their surface. In part this was one of the reasons why CNTs were chosen in this thesis as gene carriers. Because of their large surface area these materials have superior electrical carrier conductivity. CNTs have proven to be an excellent additive to impart electrical conductivity in plastics (32). Their high aspect ratio, about 1000:1 imparts electrical conductivity at lower loadings, compared to conventional additive materials such as carbon stainless steel fiber (33).

1.2.3.5 Electrical properties

Carbon nanotubes that have a chiral conformation tend to be semi-conducting in contrast with their zig-zag and chair conformations that are metallic.

CNTs have been shown to exhibit superconductivity below 20°K (34); researchers suggest that these marvelous materials, already preferred for their outstanding mechanical properties and unique ability to adopt the electrical properties of either semiconductors or perfect metals, may someday also find applications as miniature heat conduits in a host of devices and materials.

CNTs can be highly conducting, and hence can be said to be metallic. Conductivity in in some types of chair structured CNTs appear to conduct better than other metallic CNTs.

Furthermore, inter-wall interactions in MWCNTs seem to redistribute electrons over individual tubes non-uniformly.

The conductivity of single walled nanotubes has been determined by the use of electrodes placed at the ends of CNTs (35). The resistivity of the single walled nanotubes ropes was of the order of 10–4 ohm-cm at 27°C (35). This means that this material is just as effective to conduct electricity as copper, therefore these are the most conductive carbon fibers known to man. On the other hand the current density that was observed was 10-7 A/cm^2, though it's to be expected they can carry as much as 10-13 A/cm^2 (35). Being such good electrical conductors and having the capacity to arrange so much current at a time makes them ideal for electrical applications.

1.2.4 Current synthetic methods

The conditions and energy requirements to convert graphite sheets into CNTs have not been perfected yet as the current chemical vapor deposition (CVD), Arc discharge, and laser ablation methods still yield difficult to remove impurities. The amorphous carbon and metal catalyst impurities can interfere with subsequent reactions, they have been shown to change the properties of carbon nanotubes (21).

Carbon nanotubes may have been around for longer than realized as they are generated by simple carbon combustion processes in small quantities (36), though microscopy at that time was not as advance for confirmation. The first method available for CNT synthesis was arc-discharge (1). This method to produce CNTs in reasonable quantities was done by applying an electric current across two carbonaceous electrodes in an inert gas

atmosphere. This resulted in the evaporation of one electrode as cations followed by deposition at the other electrode. Both fullerenes and CNTs are formed by this method rom graphite. The

fullerenes appear in the soot that is formed, while the CNTs are deposited on the opposing electrode.

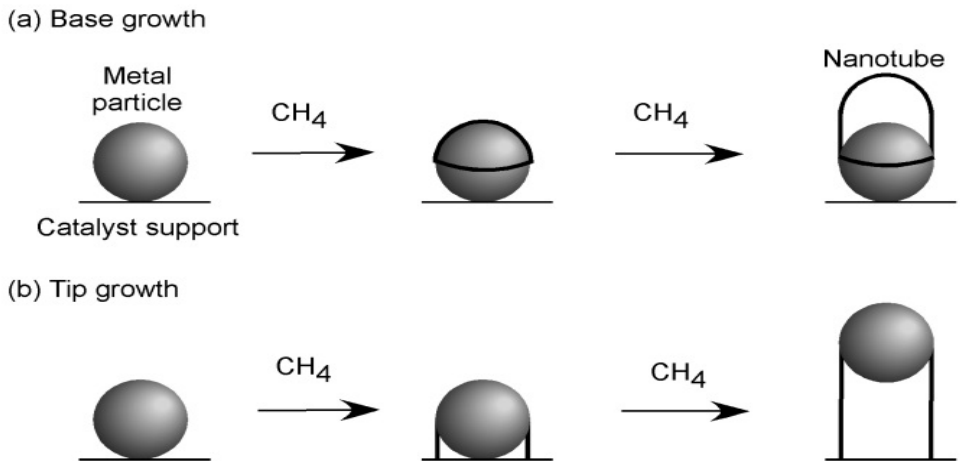

Figure 8. Two proposed pathways for nanotube growth. a) The metallic catalyst remains attached while the growth continues, while the tip growth pathway b) proposes the metallic particle travels along the growth of the tube. Methane generated from any of the synthetic pathways is shown as the carbon source.

At some point it was proposed that the CNT structures arose from the folding of a grapheme sheet. Nonetheless, this notion was quickly rejected by theoreticians. Another more suitable synthetic mechanism was proposed (Figure 8). Metallic clusters served as a surface onto which the sublimated carbon containing source deposits carbon by carbon. This would explain the fact that many CNTs are capped on one end by a held Buckyball.

1.2.4.1 Arc dischare synthesis

Nanotubes were observed for the first time in 1991 on the soot material of graphite electrodes during an arc discharge that was intended to produce fullerenes (1). This is the most common and perhaps easiest way to produce CNTs today. Nonetheless the purity of the synthetic target compound is rather low, and so further purification is required to separate from fullerene, amorphous carbon and metallic catalyst impurities.

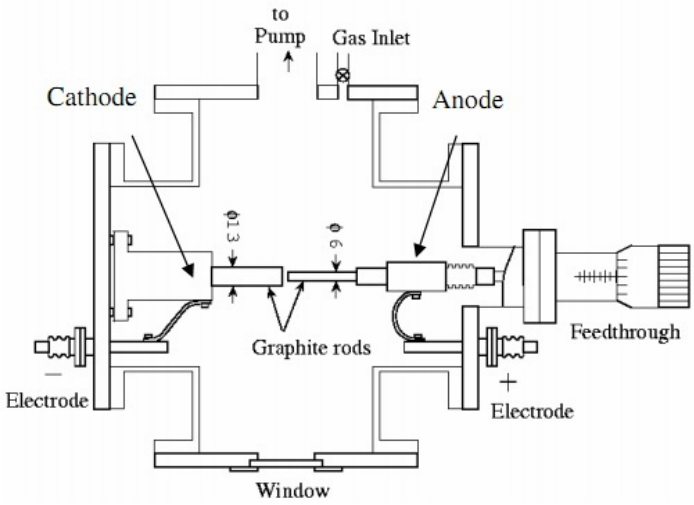

Figure 9. Schematic of the interior of an arc-discharge equipment used to synthesize CNTs. The voltage applied between the carbon electrodes produces an arc. The resulting product is collected on the cathode.

In order to synthesize nanotubes, a voltage is applied between two graphite electrodes that are separated by an average distance of 1mm. The synthetic chamber must be in an atmosphere of inert gas at a pressure of 500 torr. The energy required for transformation of the graphite electrodes is a voltage of 20–25V is applied to the electrodes with a current of 50–120 A^{o} and an arc occurs between the electrodes (37). The graphite sublimes into the plasma of the discharge forming the CNTs.

As the synthesis proceeds the tubes collect on the cathode while the anode disappears; the electrodes are moved during the experiment to keep the same electrode distance. Also doping of the electrode with metals such as cooper, iron and nickel has produced single–walled tubes (38). This method also produces other impurities such as carbon coated metal nanoparticles.The yield for this method is up to 30 percent by weight and it produces both single- and multi-walled nanotubes with lengths of up to 50 micrometers (37).

1.2.4.2 Laser ablation synthesis

This technique involved the vaporization of a graphite target with a laser in a high

temperature reactor under an inert gas. The nanotubes then condense on cool parts of the reactor. This method is more efficient than Arc-discharge for producing nanotubes in a larger scale and purity. It has been claimed that It can yield 70–90%conversion of the graphite to CNTs using this technique.(39) A schematic is shown in Figure 9, where is portrayed that the laser is used to vaporize carbon from a graphite target that has been heated in a furnace with inert gas to high temperatures(800-1,500ºC) and low pressure (500 torr).The target samples are usually prepared as 50:50 with a catalyst mixture of Cobalt and Nickel, followed by heat treatment in a vacuum at 1000°C to remove the Buckyball impurities.

Usually there is a second pulse vaporization pulse with the laser to sublimate the target more uniformly. The second laser pulse breaks up the larger particles ablated by the first one, and feeds them into the growing nanotube structure. Although the types of tube generated by this method are rope like 15nm, average diameter, and up to 100 um in length single –wall carbon nanotubes (39).

Both laser vaporization and Arc-discharge are the main methods for small scale production of CNTs. Though, both methodologies have drawbacks. In the case of arc-discharge the consumption of one of the electrodes makes it difficult for industrial scale production. On the other hand laser ablation produces highly tangled CNTs, with many impurities like amorphous carbon, metals, and other fullerenes. The CNTs thus produced are difficult to purify, manipulate, and assemble for building nanotube-device architectures for practical applications.

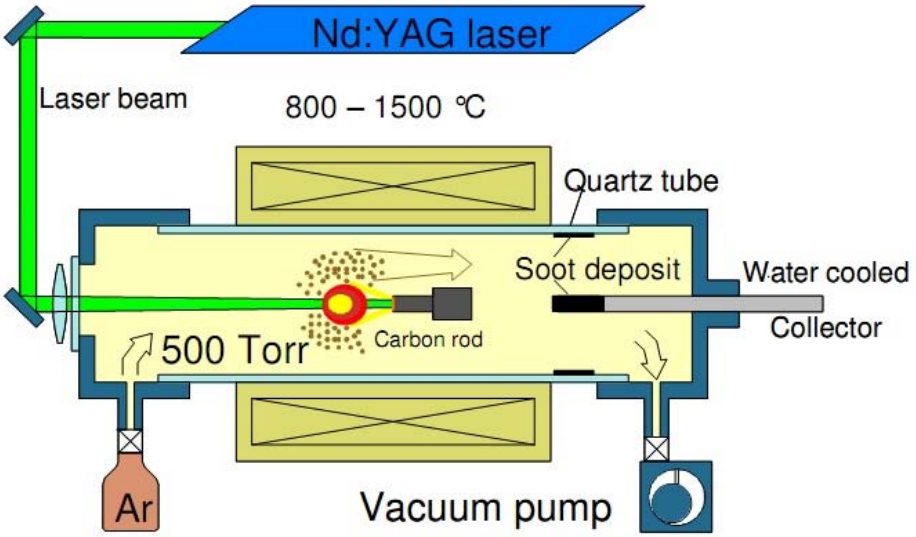

Figure10. Schematic of the interior of a laser ablation chamber. The nanotubes are formed by sublimation of a graphite substrate with a powerful laser.

1.2.4.3 Chemical Vapor Deposition (CVD) Synthesis

Chemical vapor deposition synthetic method uses catalysts to break down carbon precursors of the final product CNTs, (40-42). In the typical CVD synthesis run, a metal catalyst is heated in a furnace at a rate between 600 – 1000 ºC (41). Then the carbon containing precursors is passed over the catalyst bed to form the tubes. The reaction chamber is then cooled down in an inert atmosphere to prevent combustion of the newly formed tubes. The synthesis of single-wall CNTs using this method involves using small molecules like carbon monoxide and methane as the carbon source with catalysts like iron, nickel, cobalt and molybdenum, supported in an alumina or silica surface (41).

One advantage that CVD has over synthetic methods is the possibility to control CNT over a desired surface. Catalysts can be dispersed on a surface that is then exposed to CVD so that nanotubes grow directly on the surface, (43). Because of this trait it is hoped that these techniques will be useful in the production of field emission devices. Perhaps, if the catalyst can be patterned, it would be possible produce electronic devices such as FET so chemical sensors directly, without the need to purify or position the nanotubes first (43).

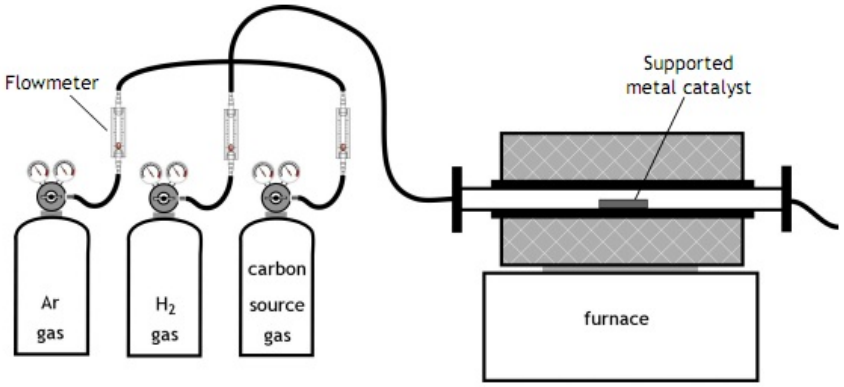

Figure11. Diagram of a chemical vapor deposition setup, this simple method is a very attractive alternative to make CNTs

1.2.5 Potential carbon nanotube applications

The impressive qualities of these hollow cylindrical molecules have caught so much attention that they have been tested in fields such as optics, nanotechnology, material reinforcement, electronics, gas storage, as well as well as applications in the medical field. They are thought of transporters due to their large surface areas, as well as their facile conjugation with other molecule through pi-pi stacking, they have been used as drug delivery systems (21). Conveniently CNTs absorb light in the transparent region of the spectrum (800-1400nm) making them ideal for photo thermal therapy (25, 26), as well as photoacustic imaging (27).

1.2.5.1 Structural support applications

Due to their outstanding hardness and flexibility, even superior to Kevlar, they are ideal materials for structural support in combination with polymers. Just as the use in silver in the clothing industry for its antiseptic properties, CNTs could be incorporated as well to produce tear resistant clothing or their use in the fabrication of bulletproof vests (44). Just as well they could become reinforcement for construction material like concrete to increase tensile strength and cracking prevention, which would save a lot of money in highway fixing programs. Just as well it could be used to reinforce our current plastics to yield more resistant furniture and automobile parts. In fact there are sports equipment using CNT to improve the quality of their items like Tennis rackets, bike parts, golf clubs and baseball bats.

1.2.5.2 Electromagnetic applications

Incredible conduction properties even superior than current metals makes them obvious candidates as chemical nanowires. By joining nanotubes end to end in the future one could envision fabricating switches and diodes at micro scale that can be used as silicon is used today in the computer industry to make computer circuits. Organic photovoltaic materials are constituted of organic semiconductors, with current CVD controlled deposition on surfaces and the semiconducting properties of them makes the ideal candidates. In fact here in UTEP Dr. Irwin is experimenting with a few carbon based materials to improve solar cell efficiency including carbon nanotubes. As mentioned previously CNTs as many other materials act as superconductors at very low temperatures. Due to their large surface area and chemical constitution they can accommodate large number of charges and therefore be used as higher efficiency capacitors

1.2.5.3 Chemical applications

These materials because of their high loading capacity could be used as molecular containers to store chemicals and be used for slow release reactions or in other areas of biotechnology. There are current research groups using CNTs for storing hydrogen. They have been found to have the potential to store 65% hydrogen by weight. If mass produced they could become important in the fuel alternative industry. Just as other allotropes of carbon like amorphous carbon they are used as filters to trap small molecules, so they could be used as water filters. They are the faster known oscillators > 50 GHz

1.2.5.4 Other applications

Just as well they have been proposed as memory materials, so regardless of the deformation they are subjected to, they will always return to their original configuration. CNTs have also been proposed as a possible gene delivery vehicle though there are mixed results regarding their toxicity using its large aspect ratio properties they have been used as carriers for many molecules from Buckyballs. Also because of its outstanding thermal dispersion properties it's been proposed to be used as heat sinks in computer motherboards.

1.3 Dynamic Light Scattering (DLS)

Polymers, particles and emulsions experience something that is called Brownian motion. This phenomenon arises from the interaction of the aforementioned particles and solvent molecules.

When such particles are exposed to a laser there is a change in in the intensity of the scattered light, which fluctuates at a rate, depended upon the size of the particles. In solution smaller particles get thrown further away by the same thermal energy of the solvent molecules compared to a larger particle. Therefore study of the intensity fluctuation upon refraction of light

elucidates the Brownian motion in a sample through the Stokes-Einstein equation.

Figure12. Picture of the Zetasizer Dynamic Light Scattering instrument used for the detection of the CNT agglomeration.

1.3.1 History

Dynamic light scattering is an instrument resulting from the discoveries made by scientist. The principal physical concept is diffusion, which is basically the thermal motion of particles through a medium. This behavior was analyzed by Fourier in the 19th century (29). Then Thomas Graham in 1833 showed the concept applied for gases and liquids in a very simple experiment. Using a hollow container containing hydrogen gas he demonstrated their diffusion out of the tube.

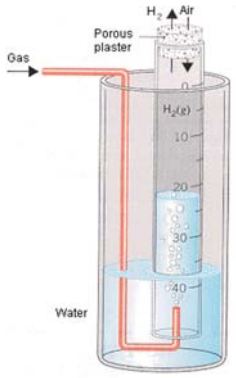

Figure 13. Thomas Graham diffusion experiment had shown an increase on the level of water in the tube that signaled the faster diffusion of hydrogen out of the tube creating a pressure difference between the system and the exterior causing the rise.

Adolf Hick using the experiments conducted by Graham he introduced for the first time the diffusion coefficient term (29). A few years earlier Robert Brown discovered that the motion of particles, in solution, is caused by their collision with other medium particles; this

phenomenon came to be called as Brownian motion. Both the discoveries of Hick and Brown settled the basis for the study of particle diffusion.

Then the work of Einstein-Smoluchowski showed that the diffusion of particles in solution was dictated by collision with solvent molecules. They also showed that diffusion was proportional to the temperature of the sample and inversely proportional to the drag constant. Finally the using the drag equation from stokes it was possible to describe the diffusion of particles in solution.

The advantage of using dynamic light scattering in my thesis is that it allows for real time measurements, it allows to measure the size change of the particles in their native environment, only viscosity and refractive index are required for measurements, it can detect very small particles, and I can use small sample volumes for measurements.

The apparatus uses a laser beam of 633 nm to determine the diffusion coefficient and the hydrodynamic radius of samples. With this light source it can detect down to 1nm particles and up to 10 um. At the same time it can determine the molecular weight of a sample down to 1000 and up to 2 E7 Daltons

1.3.2 Principles of Operation

1.3.2.1 Light scattering fluctuations

When the particles come into contact with the incident laser beam it gets refracted in all directions. If a screen were to be held close to the particle this would be illuminated by the scattered light. When you consider a system in which several particles are in solutions then you would expect an overall speckle pattern of the sample, with bright areas composed of the overall diffracted light of the particles and dark areas.

When you think down to a particle you would expect light to be refracted in all directions though when analyzing a population of such particles dark areas arise. This is explained by constructive and destructive interference of the scattered light. The bright areas therefore arise from positive interference and the dark areas from destructive interference. Of course at the same time particles have Brownian motion that dictates that smaller particles move quicker in solution compared to bigger ones. Therefore through the constant motion the speckle pattern also seems to move. This shift of dark and bright spots get recorded in the machine as light intensity fluctuations. This rate of light intensity change is used for the elucidation of particles hydrodynamic diameter.

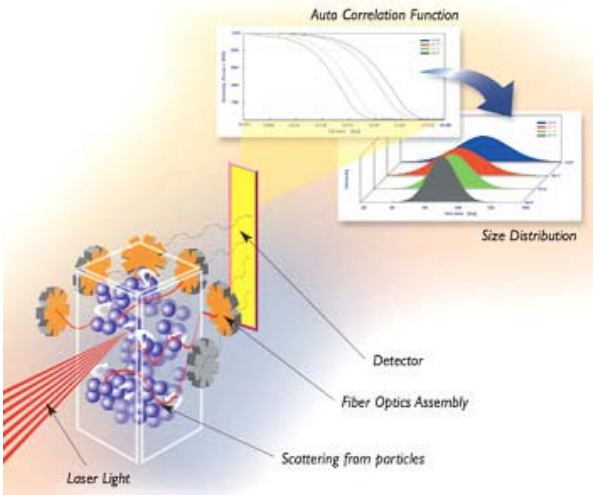

Figure 14: Dynamic light scattering uses the diffraction of the source light to detect changes, such as the in light intensity reaching the detector, resulting in the hydrodynamic radius of particles in solution.

1.3.2.2 Dynamic light scattering measurable parameters

1.3.2.2.1 Molecular weight

Using an average of over a time interval of the intensity fluctuations risen from the light scattering of the particles one can also acquire molecular weight information using the Raleight equation information.

$$\frac{KC}{R_\theta} = \left[\frac{1}{M} + 2A_2C\right]P(\theta)$$

R_θ: The ratio of scattered light to incident light of the solution.

M: Molecular weight.

A_2: 2nd Virial Coefficient.

C: Concentration of the sample.

P(θ): Angular dependent scattering intensity

K : Optical constant defined below.

$$\mathrm{K} = \frac{2\pi^2}{\rho_o^4 N_A}\left[n_o \frac{dn}{dc}\right]^2$$

N_A:Avogadro's constant.

ρ_o: Laser wavelength (633nm in this case)

$\mathbf{n_o}$: Refractive index

dn/dc Change in refractive index as a function of the change in concentration

Although there are several physical parameters that need to be known in order to calculate molecular weight, a sample can still be analyzed to acquire such information. As one can observe from the above equations scattered light collected in the DLS instrument is used along with parameters like the second virial coefficient, concentration of the sample, refractive index, laser wavelength among others to find the molecular weight of a measured particle.

1.3.2.2.2 Second virial coefficient

This instrument can also provide information about the second virial coefficient of the particles being measured. The second virial coefficient describes the strength of interaction between the particles in solution and the surrounding solvent molecules. Samples with a second virial coefficient greater that zero have particles that interact more strongly with solvent

molecules than with themselves. On the other hand samples with a second virial coefficient smaller than zero have particles that interact more strongly with themselves than with solvent molecules, and tend to aggregate.

1.3.2.2.3 Size of the particles

The particle size that is measured in a Dynamic Light Scattering spectrum is actually the hydrodynamic diameter. The obtained diameter is that of a perfect sphere that has the same diffusion as the particle being measured. As mentioned before smaller particles get thrown farther by the thermal energy of the surrounding solvent molecules. As such if you take two pictures in a short time interval like 100 us, we can determine how much the particle has moved and therefore it size. If the particle positions before and after the time interval are very similar, the particles in the sample are very large; similarly if there is a considerable change in the position of the particle then is of small diameter. In order to describe diffusion with all of these parameters taken into account the Einstein-Stokes equation was formed:

$$D_o = \frac{k_b\, T}{6\pi \cap r_h}$$

Where D_o is the Einstein-Stokes diffusion coefficient, k_b is the Boltzmann constant, T is the temperature in kelvin, ∩is the viscosity of solvent, and r_h is thehydrodynamic radius of the particles.

CHAPTER 2

2.1 Conditions of CNT functionalization

Carbon nanotubes are very resilient to chemical attack, as such very strenuous oxidation conditions have to be undertaken for Functionalization of the aromatic rings. As mentioned in the previous chapters, CNTs are amazing materials with outstanding properties, but their use is limited by their poor solubility. In order to increase the solubility of these materials without disrupting too much the surface, partial functionalization is undertaken.

2.1.1 Molecules and materials used in synthesis

Multi-wall carbon nanotubes produced by arc-discharge (Sigma-Aldrich), with an outer diameter 7-15nm and a length of 0.2-10um. Single-wall carbon nanotubes (nanomaterial store), pristine samples had an outer diameter 1-2nm and a length of 0.5-2um. Polyethyleneglycol carbon nanotubes (SWCNT-Glycol) were bought from Sigma-Aldrich. Single strand oligonucleotide sequences for sequence dependent aggregation studies were acquired from Fisher Scientific; 5'-$PC_{12}PA_{12}$-3' (Oligo 1) and PT_{24} (Oligo 2) to use in the DLS and TEM studies. Fish DNA was bought from Sigma-Aldrich for the Confocal Microscopy measurements. All of the remainder chemicals were acquired from VWR including 99% ethylenediamine, 99% thionyl chloride, sodium hydroxide, 13mm diameter/0.2um pore size syringe PTFE filters 25mm diameter/0.2um pore size syringe cellulose acetate filters, 6N hydrochloric acid, 90% Nitric acid, 90% Sulfuric acid.

2.1.2 Acid oxidation

To functionalize CNT with a myriad of different functional groups one can derive the carboxylated carbon nanotube and does further chemistry on the flexible carboxylic acid motif to further modify the surface with different molecules. Though this is easier said than done as

strong acids like sulfuric acid, nitric acid, and hydrochloric acid are needed to disrupt the aromatic system of the rings in the CNT structure. Nonetheless, the same conditions can be used to completely oxidize carbon nanotubes and destroy them, so a proven method was used to partially functionalize CNTs but keep their physical integrity (45).

2.1.2.1 Conditions

In order to disperse CNTs for more efficient homogeneous functionalization 200 mg SWCNT were sonicated for 2hrs in a mixture 1:3 of HNO_3:H_2SO_4 (5ml HNO_3 and 13.31 ml H_2SO_4), and upheld for 48 hrs. at room temperature. Once the reaction time is completed the acid solution turns to a black solution. Then the reaction flask is placed in ice and using dropwise addition NH_4OH is used for ph. neutralization. Finally the solution is filtered with a 0.22um cellulose filter and the CNTs are washed several times with water and centrifuged at 3,000 RPM. The supernatant after centrifugation was discarded and CNTs redissolved to centrifuge again several times. When the washing water gets crystalline the product was dried for 48hrs at 60 ^oC with an 80% yield.

2.1.3 Further modification

Carboxylated carbon nanotubes were further modified by reacting with different molecules to yield CNTs with different solubility. In this work the carboxylated tubes are sonicated with thionyl chloride for eight hours to yield a very reactive acid chloride intermediate after centrifugation purification. The figure on the bottom depicts the reaction type, but instead of octadecylamine like in the figure, in this work ethylenediamine were used to modify the acid chloride nanotubes in an attempt to synthesize tubes with greater dispersion properties. The resultant multiwall carbon nanotubes functionalized with ethylenediamine (MWCNT-EDA), and

the oxidized SWCNT with carboxylic acid functional groups (SWNCT-COOH) were properly purified.

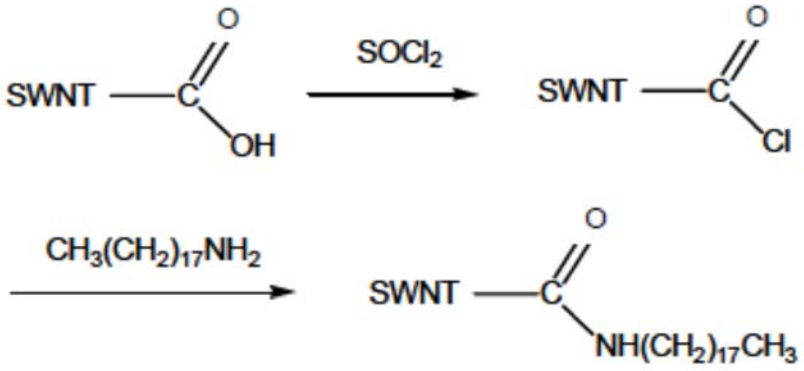

Figure 15. Further modifications of oxidized CNT to yield several varieties

2.2 Purification of CNT samples

The samples were filtered using a cellulose acetate filter and further centrifuged for contaminant separation. The removal of the supernatant was performed using a Pasteur pipette and a bulb, followed by suspending the CNTs to wash again three times and repeat procedure.

2.3Stock preparation

In order to the decrease the amount of variables in the experiments and maintain the results as constituent as possible CNT stock suspensions were prepared to be used in all measurements throughout the thesis. All suspensions were prepared in 0.5 mg/ml concentrations with water as a solvent. The mixtures were sonicated for 1 hr. straight to ensure a homogeneous mixture. This was followed by separation into several 500ul aliquots contained in eppendorf tubes. The samples were refrigerated at -20^{o}C until needed for measurements.

2.4 CNT/DNA sample preparation for solubility test

In an attempt to capture CNT/DNA complexes representative of what happens in solution the liquid samples were quickly frozen using a -80^{o}C refrigerator then lyophilized. The stock

aliquot (0.5 mg/ml, 500ul CNT samples) solution, was centrifuged for thirty minutes, and then mixed with the same volume of a Fish DNA solution (1 mg/ml) in a 2 ml eppendorf. Each sample was then incubated for thirty minutes for CNT/DNA complex formation. Then the mixture was centrifuged at 5000 R.P.M for ten minutes and the pellet was collected, followed by suspension in the same volume of water. Immediately after the mixture tubes were placed in the freezer to trap the solution conformation of the CNT/DNA aggregates. When completely solid the tops of the tubes were covered quickly with parafilm and perforated with a needle for more efficient pressure equalization. The lyophilization machines reach a pressure of about 0.1M Bar and a temperature reading of – 40ºC automatically; the samples are left for sublimation overnight.

2.5 Characterization parameters and sample preparation

2.5.1 X-ray Photoelectron Microscopy

2.5.1.1 Instrument and measurement parameters

The measurements were performed in a Perkin-Elmer Phi 560 instrument. The measurement chamber was maintained between one to three nanotorr pressure. The x-rays produced by the machine were generated by a Mg K lamp generating 15 eV impacting on Mg at 200 W. Twenty five sweeps were done per measurement and averaged to yield the final spectrum.

2.5.1.2 Sample preparation

Careful sample preparation is essential to ensure good quality data. Dried CNT samples were ground with a clean mortar for better measurements. Handling of the materials was always done with clean tweezers and gloves. The sample was dispersed on top of a copper spectra

graded tape surface to completely cover it (2 cm diameter copper circle). The powder was pressed to completely saturate the tape surface and ensure a better signal.

2.5.2 Infrared spectrometry

2.5.2.1 Instrument and measurement parameters

Samples were observed using a Thermo Nicolet (Nexus 470 FT-IR), with software package OMNIC v6.Pellets were formed using a hydraulic press after sample preparation with potassium bromide (Fisher). Before any measurement a background correction was performed. An average of sixteen scans yielded the final spectra with a resolution value of thirty-two.

2.5.2.2 Sample preparation

The powder sample and KBr was ground, in a mortar, to reduce the particle size and homogenize the mixture. Otherwise, large particles scatter the infrared beam and cause a slope baseline of spectrum. A small amount of powder sample (0.1-5% of the KBr weight) is mixed with the KBr powder. Subsequently each sample was ground until a homogeneous gray color was perceived (1-2 minutes). After the pellet was formed with a press it was placed in the infrared checking alignment with the beam and measured for transmittance.

2.5.3 UV-VIS spectrometry

2.5.3.1 Instrument and measurement parameters

UV-VIS spectra were recorded on a Perkin Elmer Lambda spectrometer using WinLab software to process the spectra. The run was recorded from 200-800nm allowed for absorption recording. The samples were measured using a one centimeter quartz cuvette to allow for exploration of spectra down to 180nm.Before any measurement a background correction was performed.

2.5.3.2 Sample preparation

Ultrapure MilliQ water was used for the UV-VIS analyses, in order to reduce contaminant presence and potential noise. In order to reach an acceptable spectrum one needs to acquire a spectrum with absorption below one. Compounds usually in the range of 10^{-3}-10^{-5} M give off this trend; as such samples containing CNTs to make a 1mM with water were prepared and sonicated vigorously for thirty minutes before measuring.

2.5.4 Nuclear Magnetic Resonance

2.5.4.1 Instrument and measurement parameters

The spectroscopic observations were done using JEOL600 MHz NMR equipment with the topspin software package. Deuterated water was bought from Sigma-Aldrich.

2.5.4.2 Sample preparation

Sample was prepared by weighting 5mg of the dried purified CNT sample. The nanotubes were sonicated for thirty minutes in 1.5ml of deuterated water to reach a height of about five centimeters in the NMR tube.

2.5.5 Raman spectroscope

2.5.5.1 Instrument and measurement parameters

The measurements were performed in a Thermo Scientific DXR instrument. The spectra were analyzed with the OMINC software for integration, height correction, and positions of peaks. The samples were excited at 780nm achieved by a diode laser. The aperture focus of that achieved the better results was 50um, and the sample was exposed for 60s.

2.5.5.2 Sample preparation

Carbon nanotubes suspensions at a concentration of 0.5 mg/ml, in 100% methanol for quick evaporation, were deposited on top of a silica wafer until the surface was completely covered. Handling of the materials was always done with clean tweezers and gloves.

3.5.6 Thermal gravimetric analysis

2.5.6.1 Instrument and measurement parameters

The measurements were performed in a Mettler Toledo TGA/DSC 1 instrument. The spectra were analyzed with the STARe software for taking the first derivative of the TGA plots and percentage of loss mass observation. The samples were slowly heated at a rate of 20 ^{o}C/min up to 600 ^{o}C to ensure good thermograms. The samples were also heated under a gas flow of 20 ml/min of nitrogen.

2.5.6.2 Sample preparation

Purified CNTs samples were loaded into a small weighting boat, and loaded as is. It was attempted to always load less than three milligrams of the sample.

2.5.7 Confocal microscopy

2.5.7.1 Instrument and measurement parameters

The instrument used was the Zeiss Pascal confocal scanning microscope equipped with four lasers and four objectives for observation. Liquid samples were loaded using common objectives and coverslips (Sigma-Aldrich). The luminescent dye 4′,6-Diamidino-2-phenylindole dihydrochloride or DAPI was from Sigma-Aldrich as well.

2.5.7.2 Sample preparation

Carbon nanotube aliquot suspensions with 0.5 mg/ml concentrations were removed from the fridge and sonicated for thirty minutes. The homogeneous samples were then transferred with a Pasteur pipette onto a glass slide and topped with a coverslip for observation.

Samples for the observation of CNT/DNA complexes were prepared with DAPI dye. In order to visualize the interaction between CNTs and DNA dye markers are needed. Because of the high efficiency and specificity DAPI dye was chosen with a 405 excitation and a 450 nm emission wavelength. A DAPI solution was prepared from the DMSO stock solution to dilute to a final concentration of 1 ug/ml DAPI (Invitrogen D1306)(stock 1 mg/ml in water, store at -20^{o}C; 10 ul for 10 ml final).

The stock aliquot (1 mg/ml, 500ul CNT samples) solution was sonicated before used for thirty minutes at room temperature. A 500ul solution of a Fish DNA solution (1 mg/ml) in a 2 ml eppendorf was incubated with 20ul of the prepared DAPI solution, and incubated at room temperature for thirty minutes. To allow for the mixture to reach equilibrium, thirty minutes of incubation time was determined to be ideal. Then the mixture was centrifuged at 5000 R.P.M for ten minutes, followed by removal of the supernatant using a Pasteur pipette and bulb, followed by suspending the CNTs in the same volume.

2.5.8 Transmission Electron Microscopy (TEM)

2.5.8.1 Instrument and measurement parameters

Pictures were taken using a Hitachi H-7650 microscope with an accelerating voltage of 40-120 kV, and a resolution mode reaching 600,000X. The samples were loaded, onto Polyscience, Inc., coated nickel 300 mesh grids to prevent CNTs from going through.

2.5.8.2 Sample preparation

Carbon nanotube aliquot suspensions with 1 mg/ml concentrations were removed from the fridge and sonicated for thirty minutes. Then using a mechanical pipette the samples were transferred to the coated grids as solutions and allowed to dry. Five drops of 20ul each were allowed to evaporate on the surface of the grids for each sample.

2.5.9 Scanning Electron Microscope (SEM)

2.5.9.1 Instrument and measurement parameters

Observation of the samples was done using a Hitachi H-7650 microscope with an accelerating voltage of 15 kV Hitachi, and the elemental analysis was done with theS-4800 *SEM* EDAX Pegasus XM4. The samples were loaded onto 3M^{TM} adhesive conductive copper tapes as a solution. Once the water evaporated from the grid the samples were introduced into the system.

2.5.9.2 Sample preparation

Carbon nanotube aliquot suspensions with 1 mg/ml concentrations were removed from the fridge and sonicated for thirty minutes. Then using a mechanical pipette the samples were transferred to the coated grids as solutions and allowed to dry.

2.5.10 Dynamic Light Scattering specifications

2.5.10.1 Instrument and measurement parameters

The measurement instrument used to generate the results presented in this thesis is the model Zetasizer nanoS, with a 633 nm laser, from Malvern Instruments Co. The samples were placed on 1 cm quartz cuvettes.

When measuring the samples viscosity and refractive index values for water at twenty five degrees Celsius were used. The medium in which the light travels is obviously of great importance as both previously mentioned parameters will have an effect on the speed of the traveling light and the directionality. In this case the parameters used were 0.8872 cP for viscosity and 1.33 for the refractive index. To gather more valuable information from this fluid measurement one minute time was provided of equilibration time before the instrument gathered any information. Just as important the measurement was setup to present a final assessment of

the average of six measurement runs containing three cycles of ten second each. This of course in an attempt to improve the quality of measurement presented.

Every time measurements were recorded a background spectrum was collected as well as our controls. The instrument though very powerful is limited to measure particles from 0.3nm to 10um, and sample concentrations down to 0.1 ppm to 40% w/v.

2.5.10.2 Sample preparation

Water treatment for noise reduction

Thorough treatment of the water used for the preparation of the samples was carried out to remove completely of DNAses and dust particles. Water was collected from milliQ filtration systems and distilled on thoroughly rinsed glassware, in an attempt to isolate the condensed water from the dust in the air. Later the water was filtrated, and collected in clean glass bottles. The final step before storing involved the autoclaving of the water filled bottles to denature any remainder DNAses. Before using the water the desired volume was removed in a hood and transferred to Eppedorf tubes for centrifuging at 5000 R.P.M for fifteen minutes.

Carbon nanotube control preparations

The solutions for DLS measurement were prepared by weighting the dried CNTs samples after purification. The numbers of milligrams measured in a five significant figure balance were dispersed in the same amount of milliliters to make 0.5 mg/ml suspensions. The samples were sonicated for thirty minutes before each use.

Carbon nanotube and ionic solutions

The purpose of this exploration was to determine the behavior of CNTs in Saline-sodium citrate buffer (SSC), a very good buffer for DNA hybridization. Therefore CNTs controls were

prepared as instructed, but 20ul of a 50X SSC buffer to a 1ml control solution was observed for behavior.

Carbon nanotube/DNA molecular ratio

Complementary ssDNA sequences were bought from Fisher Scientific, the first oligonucleotide sequence contains a mix twenty-four nucleotides; 5'-$PC_{12}PA_{12}$-3' (Oligonucleotide 1). The second complementary sequence is a oligomer made of twenty-four nucleotides thymine; PT_{24} (Oligonucleotide 2). In this experiment using aggregation DNA sequences the ideal molecular ratio of CNTs/ DNA was searched. As such, ratios of one to one, one to ten, and one to a hundred CNT/DNA with excess DNA were studied.

2.6 Results and Discussion

2.6.1 Functionalization of carbon nanotubes

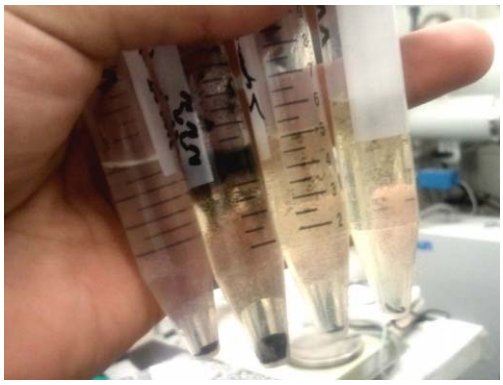

Figure 16. Centrifuge tubes with carbon nanotubes in the middle of a purification procedure

Carbon nanotubes are large enough that they can be easily precipitate by centrifugation. Being that there is a radical difference in solubility between functionalized CNTs and pristine tubes, it's expected that most commonly used purification methods undertake physical separation of products and contaminants. In the picture above, a batch of Osorio's oxidation method is

shown, in which the pellet contains the modified CNTs and the yellowish supernatant the salts generated by the acids in the reaction mixture.

Figure 17. Comparison of pristine CNTs and the carboxylated carbon nanotubes

When enough washes and centrifugation cycles are performed the supernatant is no longer yellowish signaling complete removal of salt contaminants. This followed by cellulose acetate filtration ensures the isolation of only the water soluble CNTs. Once carboxylated and purified, as shown in the picture on top, it yield much more stable suspensions than pristine CNTs. In fact, the reaction batch in the picture was over three months old.

2.6.2 Functionalized carbon nanotube (f-CNT) solubility

Since the purpose of this thesis is the generation of a nanotube gene sensor that can be detected, through quick and inexpensive, DLS measurements, the utilization of different sized tubes must be explored. Carbon nanotubes as shown in most SEM and TEM imaged tend to bundle together through strong Van Der Wall interactions. Therefore the more stable the suspension the slower the aggregation behavior, so the need to try different water soluble motifs to modify the surface of CNTs; PEG and ethylenediamine.

Another method to increase solubility of CNTs is using surfactants and molecules that adhere to the surface of the tubes to improve transport in aqueous media. Interestingly Toita, et

al. demonstrated that solubility of CNTs could be greatly improved with DNA alone (46). As such pristine CNTs were used in this thesis as well.

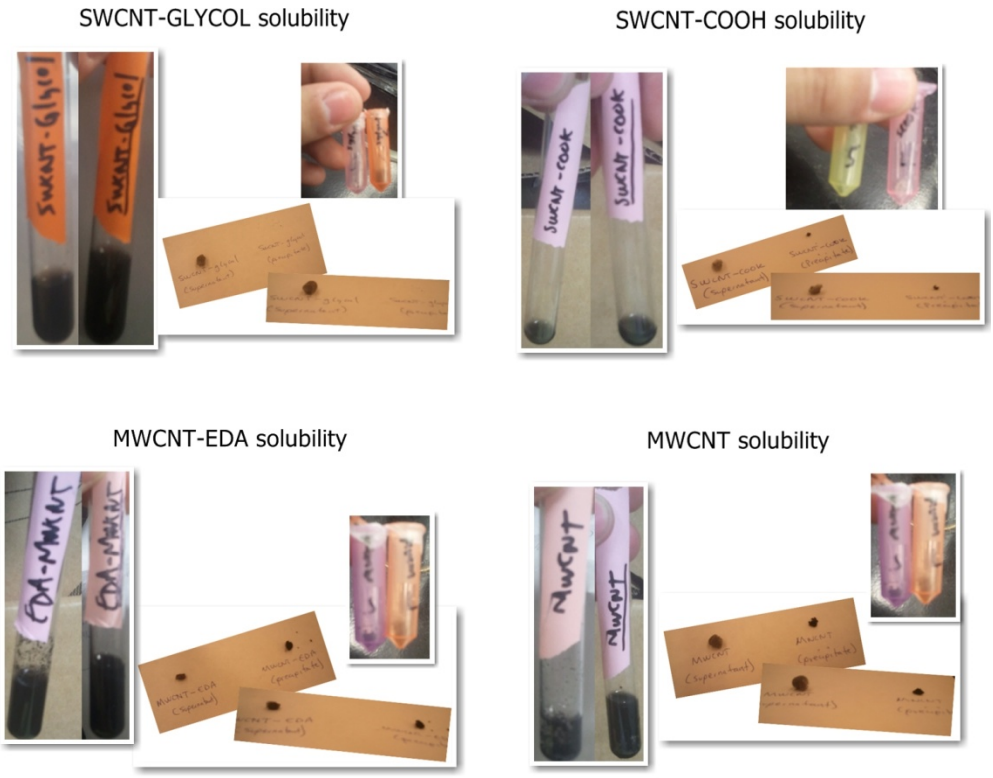

Figure 18. Pictures taken to appreciate the differences in solubility of the f-CNTs

In the picture on top one can observe a set of tubes, solid samples on paper, and eppendorf tubes for each of the four types of nanotubes chosen for analysis in this work. The tube on the left is the sample with the suspended CNTs (0.5 mg/ml), and the tube on the right after addition of DNA. It's very difficult to perceive by looking directly at the tubes, but DNA samples are more disperse. Although all samples are soluble in water to a certain extent not all form good suspensions. To showcase the difference in solubility upon DNA addition, the DNA/CNT samples were centrifuged. The rectangles on the picture are pieces of paper with two black dots; on the left and right edges. The left black CNT sample is the lyophilized supernatant of CNT/DNA aggregates and the right sample, the precipitate. One can the clearly observe that

although all samples yield soluble CNT/DNA complexes (left black dot), not all samples generate the same amount of precipitate, revealing that the most ideal candidates for experimentation seem to be the nanotubes with the carboxylic acid and the polyethylene glycol motifs.

2.6.3 UV-VIS characterization of f-CNTs

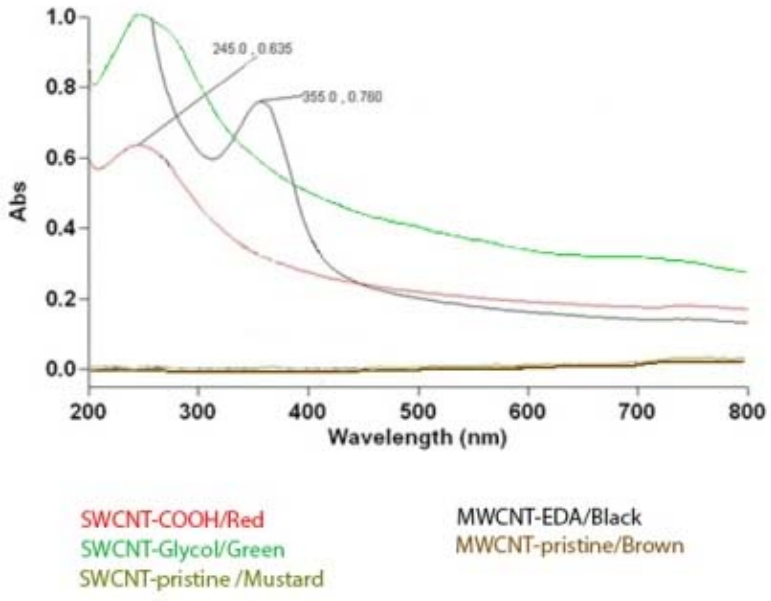

Figure 19. UV-VIS comparison of the different f-CNT

The above spectrum is proof that the functionalized CNTs do in fact solubilize in water. The UV-VIS spectrum reveals absorption peaks corresponding to electron excitation of electron on molecular orbitals. Therefore, the addition of functional groups to CNTs should introduce a new electronic environment and therefore shifts in the absorption peaks. Once can observe a maxima of 355nm for the MWCNT-EDA sample, arising from the basic nitrogen atom. Though not visible both the carboxylated and the glycosylated nanotubes have the same maxima from their carbonyl groups. Finally, one can observe that the pristine SWCNT sample does not record an absorbance due to lack of solubility. The changes in the electronic structure of SWCNTs

arising from covalent modification have been probed mainly by optical absorption spectroscopy. These studies revealed an increasing deterioration of the π-conjugated system of the tubes with rising degree of functionalization (49).

Sigma excitations from aromatic systems, alcohols, ethers, and primary amine to sigma star or antibonding orbitals occur in the far ultraviolet region below 200 nm. Nonetheless, one can clearly observe the carbonyl n-π^* transition peak for all samples coming from the excitation of an oxygen nonbonding electron and the pi-antibonding of the carbon in the carbonyl. An extra peak appears at 355 nm, which corresponds to the transition n-π^* between a non-bonding electron in nitrogen and a pi-antibonding orbital on an amine ester, that gives supporting information of covalent attachment of amine not just mere adsorption (49).

2.6.4 X-ray Photoelectron Microscopy

X-ray Photoelectron Microscopy also known as XPS is a quantitative spectroscopic technique used for the characterization of certain materials. This technique allows for the characterization of the surface of materials. It can tell you the presence of certain atoms in the surface on to what atoms are they bound to. By giving a reading of the binding energy of the excited electron it give also strong evidence on the energetic of different molecules.

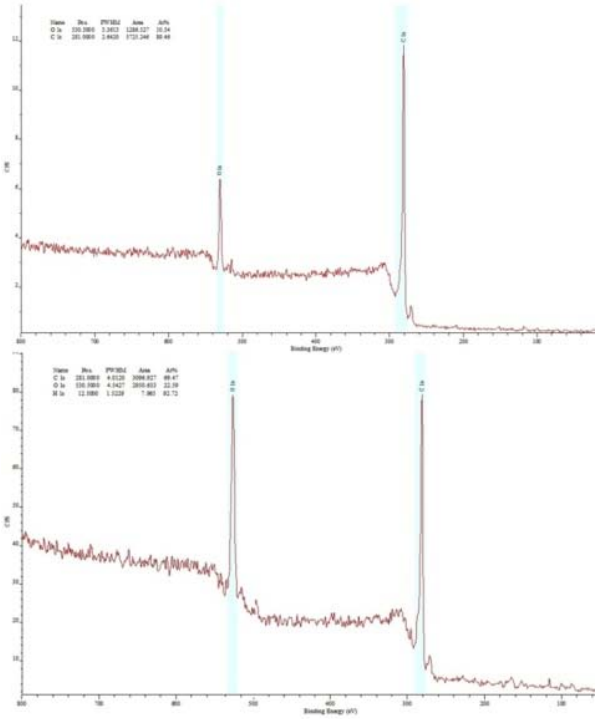

Figure 20. XPS spectra of pristine single-wall CNTs and SWCNT-COOH

The spectrum on top corresponds to pristine SWCNT, which shows two distinct peaks at 280 eV and 530 eV. The peak at 280eV is consistent with the excitation of one of the 1S electrons of the carbon atom. The peak at 530 eV is matched with a 1S electron from the oxygen atom. Comparing the 1S electrons on the oxygen and carbon, the electrons in oxygen would be subjected to the attractive force of eight protons and only to six protons in carbon. Therefore it makes perfect sense for the oxygen to have a peak at higher energy. Upon closer examination one can observe that the carbon peak is about three times bigger than the oxygen peak. This fact indicates a greater abundance of carbon atoms in the pure sample.

Although CNTs are cylindrical sp2-carbon frameworks, the truth is that current purification methods yield tubes with defects. As previously mentioned one of the methodologies for carboxylation of the surface of CNTs is acid treatment. Just as well the preferred method of purification for companies is acid treatment to completely oxidize amorphous carbon impurities and removal of metallic impurities by generation of removable salts and hydrogen. Though

conditions are not specific for impurity removal, but also for functionalization, which makes time of exposure essential to maximize impurity removal and diminish chemical modification of the pristine CNTs. Therefore is expected for the oxygen and carbon signals to appear in the XPS spectrum to signal the presence of the carboxyl functional group.

The spectrum on the bottom is the sample treated with the Osorio's oxidation method for functionalization (45). This spectrum has the same two absorption peaks at exactly the same positions for the carbon and oxygen atoms. Through a closer look one can see that the abundance of the oxygen atoms is much greater being almost the same as that of carbon. As such, one can clearly observe an increase in the carboxylic acid functionally groups in the surface of the CNTs. Increase in the surface functionalization of pristine CNT samples, as specified earlier, increases greatly the suspension stability in water.

2.6.5 Infrared spectrometry

The spectra of the functionalized CNTs confirm the presence of the expected chemical groups. Most of the functionalized samples contain strong signals confirming the surface modification of CNTs. In order to extract as much information as possible from the spectra we closely analyze each one.

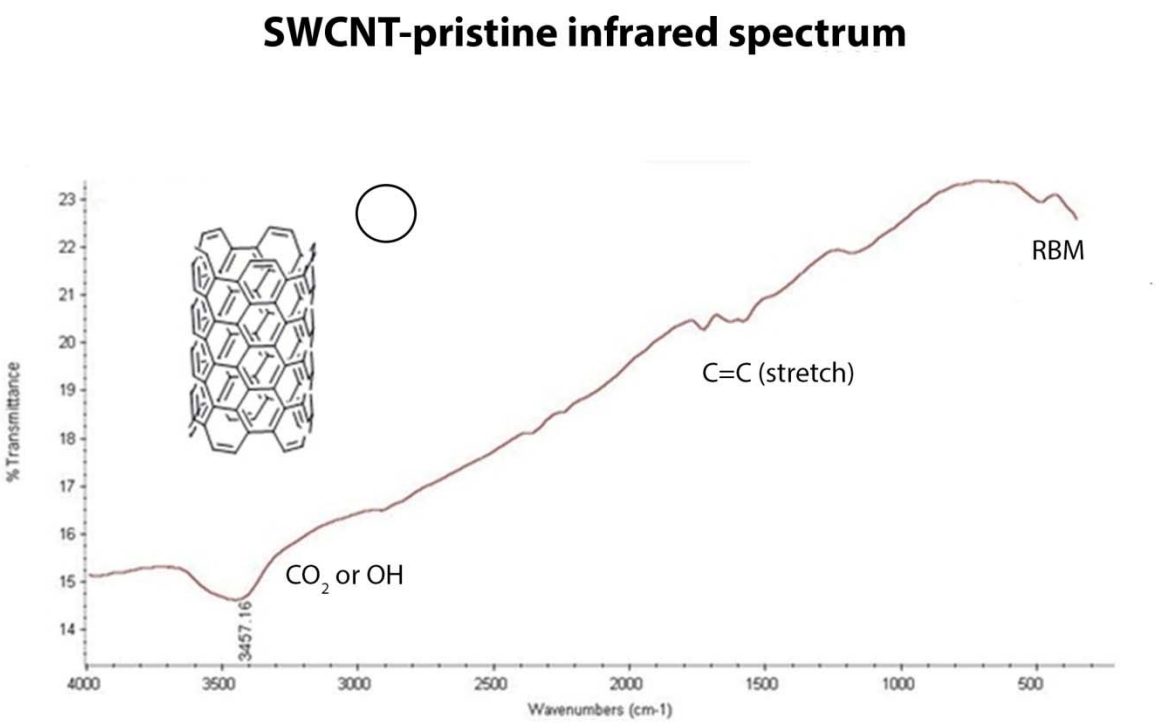

Figure 21. Infrared spectrum of pristine single-wall CNTs

In the case of the pristine sample of single wall CNTs, one can see a signal at 1600 cm^{-1}, which corresponds to an alkene carbon-carbon stretching signal. As previously stated, CNT purification introduces defects on the surface of the tubes, as well as O-H and COOH functionalization to a lesser extent. As such, the signal at 1600 cm^{-1} may be the overlap of both C=C with the O-H bending signal in the same region. The spectrum also shows a strong peak at 3600 cm^{-1}, corresponding to the O-H stretch, which supports the presence of mild functionalization. In the far infrared region one can observe a small peak, which is most likely a Radial Breathing Mode (RBM) of the tube (47). RBM modes refer to the radial expansion of the tube and relaxation, and as seen in the spectrum this is achieved at lower energies.

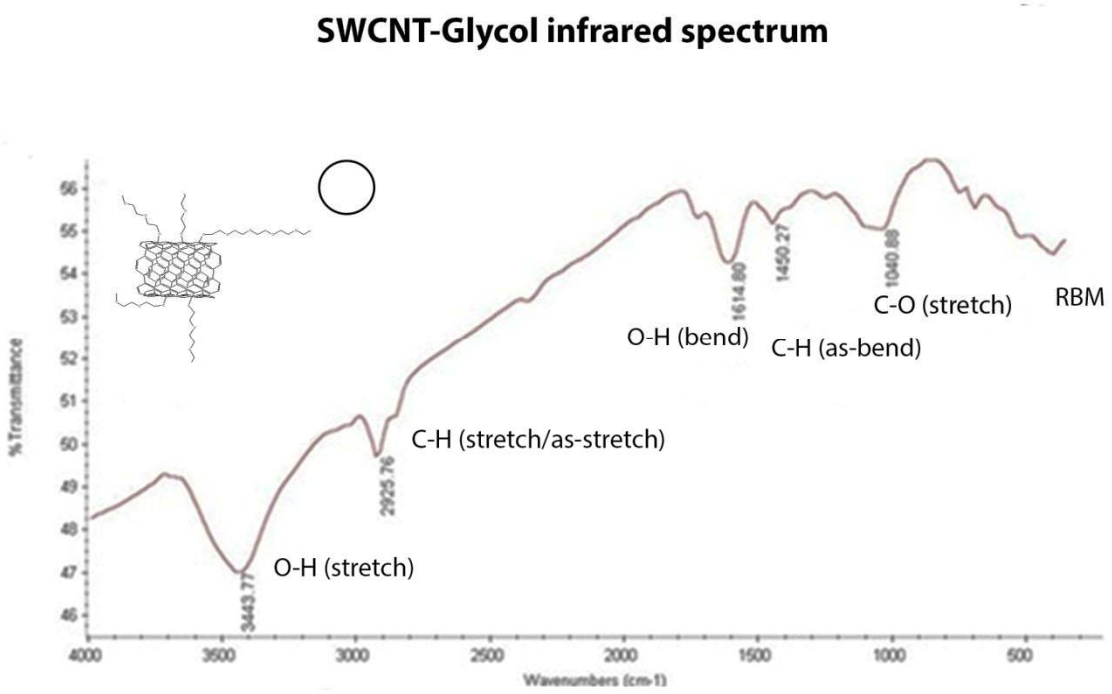

Figure 22. Infrared spectrum of single-wall CNTs functionalized with the polyethylene glycol molecule

The glycosylated single wall CNT shows the presence of a lot more peaks in the mid-IR region showcasing functionalization. Infrared signals arise from dipoles in molecules, as such is a perfect technique for functional group characterization. Nonetheless, CNTs don't have static dipoles moments and therefore pristine samples yield very small signals. The stronger intensity of the peaks is a strong indication of functionalization. The peaks from 1000-1600 cm^{-1} are characteristic of polyethylene glycol (PEG). Specifically, the signal at 1042 cm^{-1} comes from the C-O symmetric stretch of the ether functional group. Methylene group presence is confirmed by the C-H asymmetric bending absorption at 1450 cm^{-1}. This PEG signature is finished by the signal at 1614 cm^{-1} matching the O-H bending peak. The alcohol groups at the end of the PEG chains are confirmed by the very strong peak at 3443 cm^{-1}. At 2925 cm^{-1} you can also see a peak with two shoulders, the higher wavenumber shoulder corresponding to the symmetric stretching

of C-H, and the lower wavenumber shoulder corresponding to the asymmetric stretching of the C-H signal. Finally, the RBM seems to be less intense than in the pristine sample.

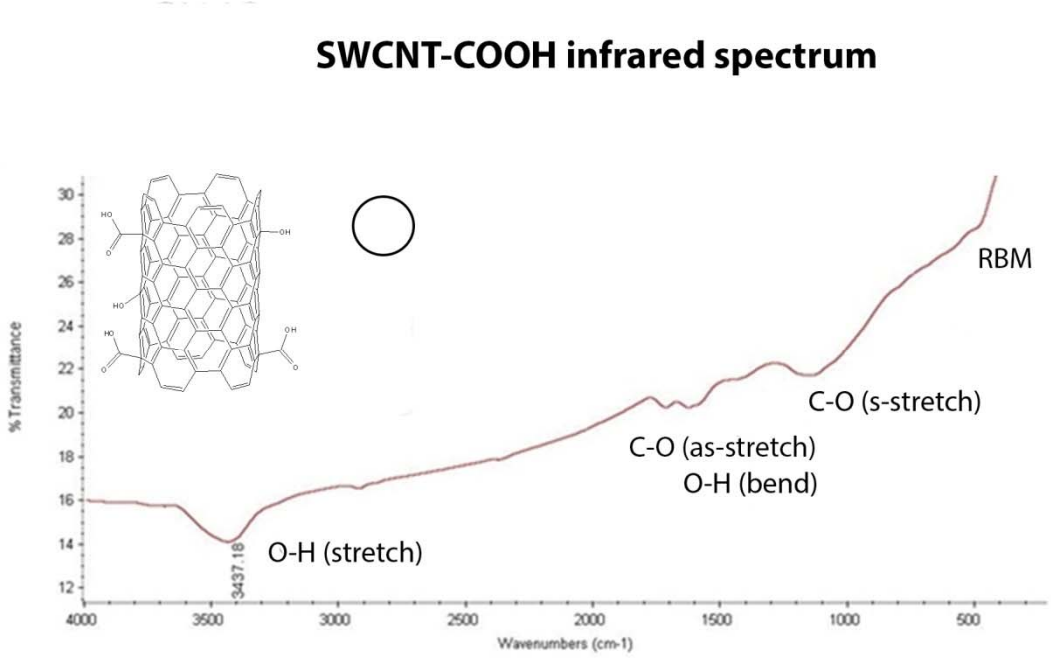

Figure 23. Infrared spectrum of single-wall CNTs with the carboxylic acid functional group

The sample subjected to oxidation by addition of $HNO_3/HCl/H_2SO_4$ appeared to have introduced a small degree of functionalization. The spectrum is in fact very similar to the pristine sample with the more pronounced C-O symmetric stretch at 1100 cm−1, which would suggest higher carboxylic acid presence just based on intensity. Also the asymmetric stretch of the C-O is spotted at 1700 cm^{-1}. The spectrum also shows the bending and stretching peaks of O-H at 1600 and 3400 cm^{-1}. RBM doesn't appear to be as strong as in the pristine spectrum. The spectrum of this water soluble CNT is not very different from the non-functionalized commercial sample.

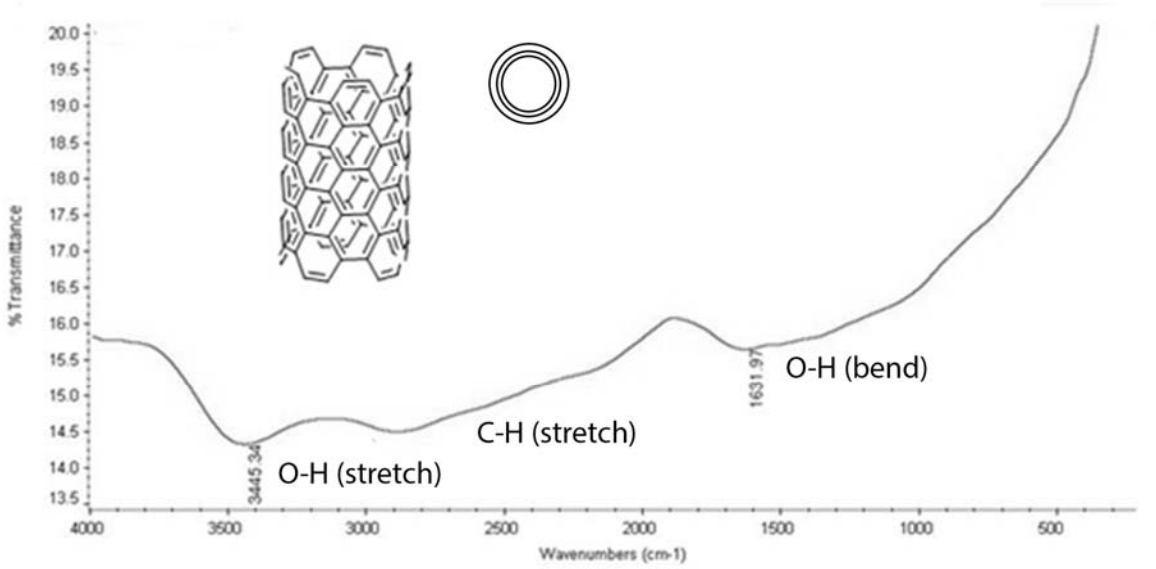

Figure 24. Infrared spectrum of pristine multi-wall CNTs

In the case of the pristine sample of multi wall CNTs, one can see an odd spectrum that contains and extra peak at 2700 cm^{-1}. Presence of defects in the surface of CNTs is not rare in purified samples, and the signal at 2700 cm^{-1} corresponds to the C-H stretching signal, which can signal the presence of defect sites (48). You can still see the bending and stretching peaks for O-H group at 1631 and 3445 cm^{-1}. In contrast with SWCNT you can clearly see the absence of RBM, which through the restriction of internal and external tubes make total sense. This radial movement restriction will then prevent dynamic dipole moments found in SWCNT, which might attribute for the odd spectrum.

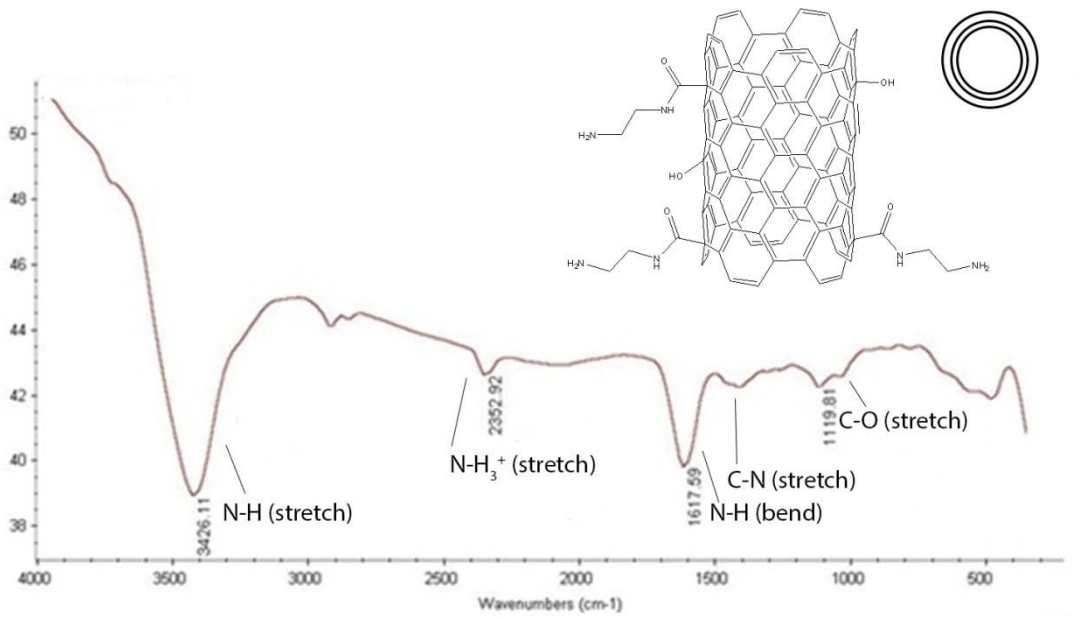

Figure 25. Infrared spectrum of MWCNT functionalized with ethylenediamine molecule

This sample shows a perfect spectrum, although compared with the other functionalized tubes it doesn't form as stable suspensions in water. Firstly, one can observe a sharp strong peak at 3426 cm^{-1} that is characteristic of N-H stretch. This functional group is the confirmed through the peaks at 1617 and 1400 cm^{-1}, which correspond to N-H bending and C-N stretching peaks respectively. This carbon nanotubes sample seems to protonate forming ammonium groups as shown in the 2352 cm^{-1} N-H stretching specific for ammonium ions. Finally the signal at 1119 cm^{-1} shows the presence of ester groups, which is proof of functionalization.

2.6.6 Raman spectroscopy

Another very powerful characterization technique for CNTs is Raman spectroscopy. Since infrared peaks appear when there is a change in dipole moments in molecules is not a very efficient technique for CNTs. Raman instead induces these dipoles making measurement possible for non-polar molecules like CNTs.

Spectra can reveal degree of functionalization, diameter of tubes, amount of impurities, as well as revealing the integrity of the sp2 system. In the case of SWCNT one can determine the diameter of the nanotubes with the frequency of the peaks below 500 cm^{-1} by using CNT ν_{RBM} = 234/d + 10 for SWNT (50). These absorbance peaks correspond to the radial breathing modes (RBM), of the carbon nanotube, which refer to the radial expansion and contraction of the tubes. The peak around 1500 cm^{-1} is know as the G-band or the tangential mode of the tube, which is due to stretching of the sp2 carbon along the length of the tube. The peak around 1300 cm^{-1} is known as the D-band or is also known as the disordered band, which corresponds to the stretching of sp3 carbons. As such, the ratios of the G-band and D-band intensities gives information regarding functionalization degree, I_D/I_G (51). The region between the G and D bands is important, as the greater the intesity im the region the greater the content of amorphous carbon impurities (52).

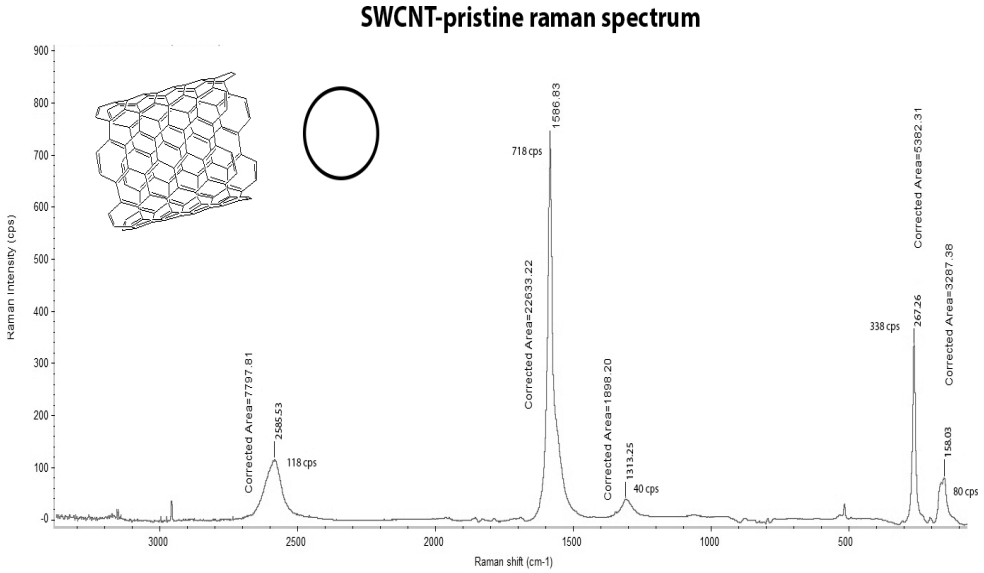

Figure 26. Raman spectrum of SWCNT-pristine molecule

The SWCNT pristine sample spectrum shows that the sp2 stretching G-band is located at 1586.83 cm-1, and the sp3 stretching D-band is found at 1313.25 cm^{-1}. The intensities for the bands are 40 counts per second (cps) and 718 cps, respectively. As such the I_D/I_G = 0.0557 confirms that the pristine sample is not a perfect sp2 system, but it's functionalized and contains defect sites by 5.7%. Small amorphous content is show due to baseline raise between G and D-band, but very little. Diameter is determined by using $\nu_{RBM} = 234/d + 10$ for SWNT and the frequencies in wavenumber found at 267.26 and 158.03 cm^{-1}. The radial mode peaks reveal populations of tubes with diameters of 0.9 and 1.6nm. Finally the G' band is located at 2590.75 cm^{-1}.

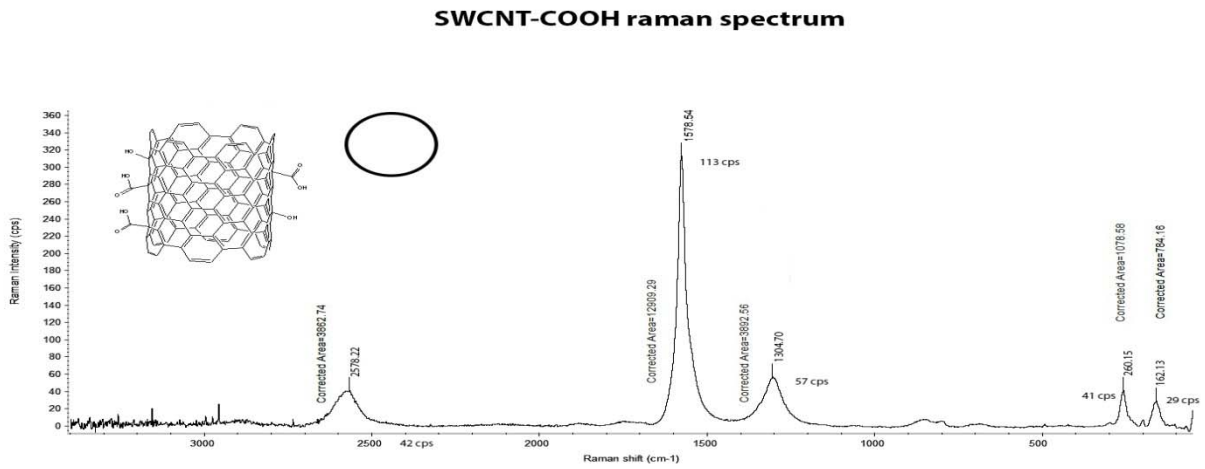

Figure 27. Raman spectrum of SWCNT-COOH molecule

The SWCNT-COOH sample spectrum shows that the G-band located at 1578.54 cm-1, and a D-band at 1304.70 cm^{-1}. The intensities for the bands are 57 cps and 113cps, respectively. As such, the I_D/I_G = 0.5044 showing that taking into account the ratio for the pristine sample reveals 44.37% functionalization. This compared to the pristine SWCNT sample contain more amorphous content. Since the same CNTs were used for functionalization the diameters are kept constant, which is confirmed by the RBM peaks in the spectrum. You can observe a shift in the G-band of 8.29cm^{-1}, compared to pristine sample, suggesting that there is a weakening of the sp2

system on the tube as you need less energy for tangetial stretching. Then you can also observe a G' band shift of 12 cm^{-1}, which is supporting evidence for functionalization.

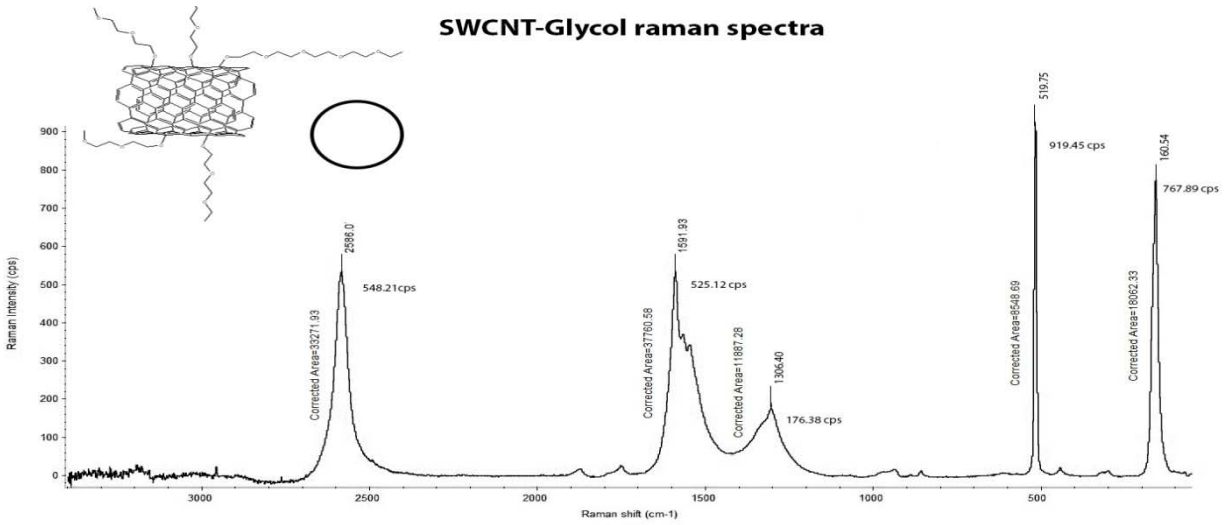

Figure 28. Raman spectrum of SWCNT-Glycol molecule

The SWCNT-glycol sample spectrum shows that the G-band located at 1591.93 cm-1, and a D-band at 1306.40 cm^{-1}. The intensities for the bands are 176.38 cps and 525.12 cps, respectively. As such, the I_D/I_G = 0.335 showing that taking into account the ratio for the pristine sample reveals 27.8% functionalization. This sample contains the most amorphous carbon impurities of all of the SWCNT derivatives used in this thesis. These tubes were bought from Sigma-Aldrich, as such the SWCNT source is different. RMB peaks CNT populations of 0.5 and 1.6nm in diameter. You can observe a shift in the G-band of 5.1cm^{-1}, compared to pristine sample, suggesting that there is a weakening of the sp2 system on the tube as you need less energy for tangetial stretching.

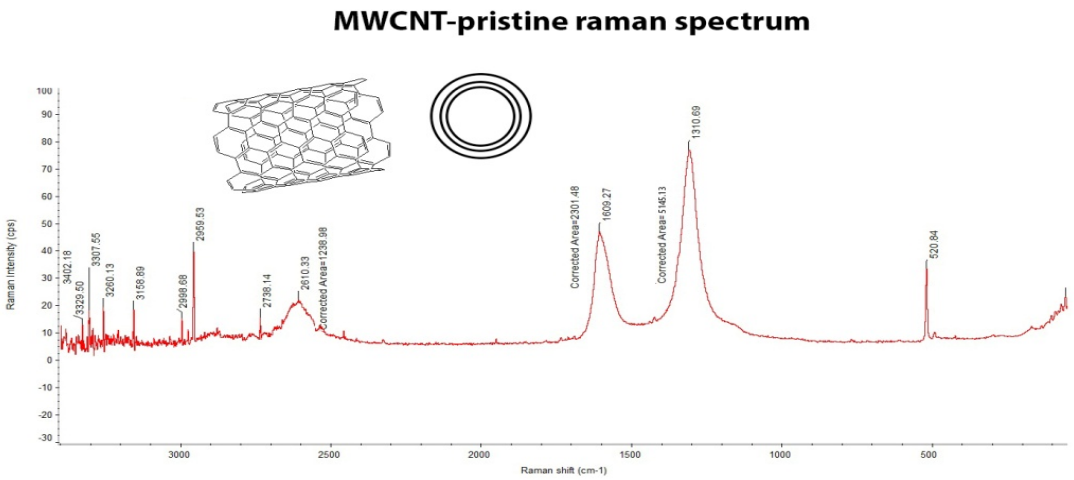

Figure 29. Raman spectrum of MWCNT-pristine molecule

The MWCNT pristine sample spectrum shows that the sp2 stretching G-band is located at 1609.27 cm-1, and the sp3 stretching D-band is found at 1310.69 cm^{-1}. The intensities for the bands are 65.37 cps and 38.74 cps, respectively. As such the I_D/I_G = 1.73, which suggest a nanotube with small degree of carboxylic acid functional groups, as show in IR, and several defect sites (53). Considerable amorphous content is show due to baseline raise between G and D-band. Since MWCNTs are concentric single-wall nanotubes, one can expect them to be more rigid SWCNTs and therefore don't contain radial breathing modes. Finally the G' band is located at 2610.33 cm^{-1}.

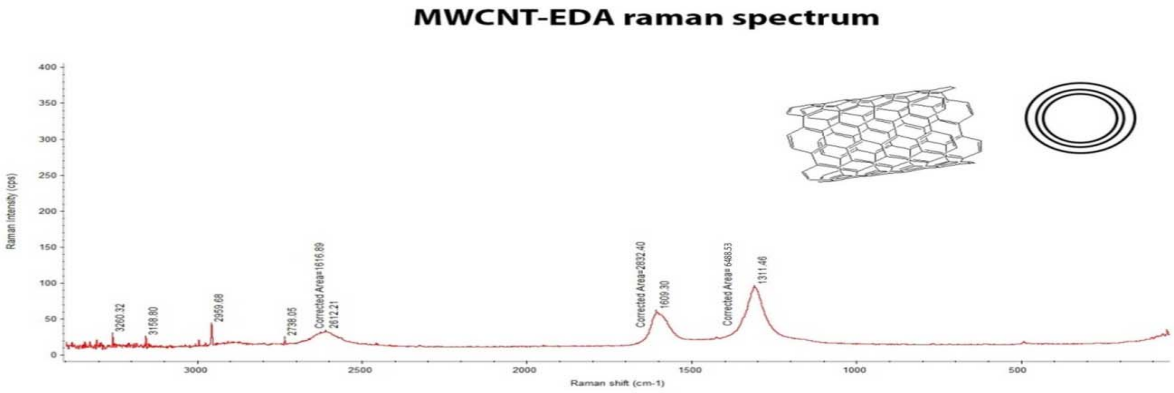

Figure 30. Raman spectrum of MWCNT-EDA molecule

The MWCNT-EDA sample spectrum shows that the G-band located at 1609.30 cm-1, and a D-band at 1311.46 cm^{-1}. The intensities for the bands are 69.88 cps and 35.23cps, respectively. As such, the I_D/I_G = 1.97 showing that taking into account the ratio for the pristine sample reveals 12% functionalization. This makes a lot of sense since them sample show to improve its solubility properties very little, even though the IR showed the presence of ammonium ions. This compared to the pristine MWCNT sample contain about the same amorphous carbon content. Then you can also observe a G' band shift of 1.88 cm^{-1}, which is supporting evidence for functionalization.

The analysis of the CNTs samples revealed that from the SWCNT samples the SWCNT-glycol sample contained the highest amount of amorphous carbon followed by SWCNT-COOH, and finally the pristine sample. It also showed diameter distributions of 0.6, 0.9, 1.6nm with 5.7%-44.7% functionalization. The MWCNT samples shown to have a greater number of defect sites, and also it was shown 12% functionalization for the MWCNT-EDA sample.

2.6.7 Thermal gravimetric analysis

Thermal gravimetric analysis aside from giving information on the thermal stability of compounds it relates it to mass loss in a sample. Although we can't get exact values, we can certainly see behaviors that relate to purity of a sample, temperature stability, and helpful in compositional analysis. Metallic impurities leftover from the synthetic reaction of CNT samples leads for catalytic decomposition of CNT in oxidative environments, as such in order to get a more reliable TGA plot the experiment was conducted in nitrogen (54).

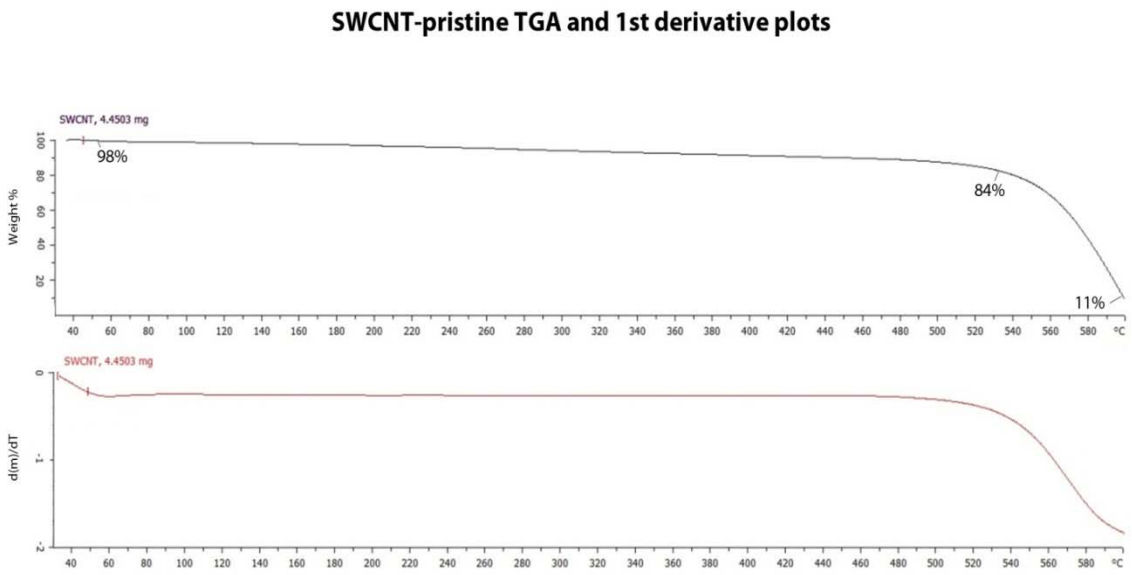

Figure 31. Thermal gravimetric analysis and DTG plots of SWCNT-pristine molecule

In the case of the pristine SWCNT, the curve shows an immediate loss mass that is barely visible in the TGA plot, but becomes much more apparent in the DTG curve (1st derivative of TGA curve), this corresponds to loss of trapped water inside CNTs (55). In accordance to the amount of functionalization shown through Raman (5.7%), one cannot distinguish another distinct curve, in the TGA plot, before it reaches the decomposition temperature of the CNTs. Nonetheless, it seems pretty obvious that there is a steady decrease in mass from 70-520 ºC, which can be attributed to the mass loss of the less stable amorphous carbon impurities. Finally the pristine CNT sample with 5.7% defect sites shows a thermal stability up to 520 ºC, after when mass loss continued until the temperature ramp was stopped. The sample at 600 ºC shows a final mass of 0.489 mg (11% of the initial mass), which is very near to what researchers have found with other CNT samples (56). This remaining mass can be attributed to the catalysts metallic particles leftover.

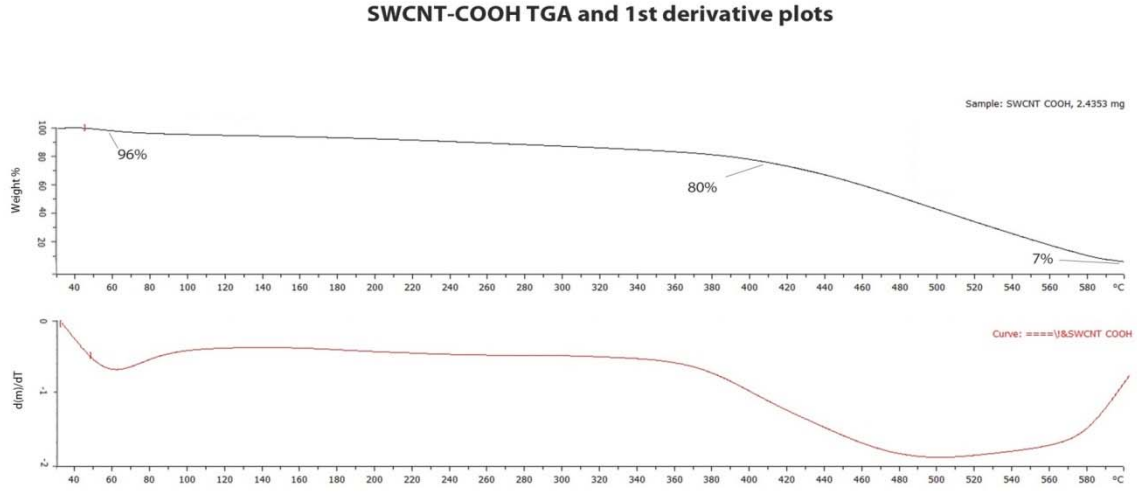

Figure 32. Thermal gravimetric analysis and DTG plots of SWCNT-COOH molecule

The SWCNT-COOH curve, in contrast with the pristine sample, shows decrease thermal stability of the CNTs, and greater mass loss before reaching CNT decomposition temperature. The initial mass peak, as shown in both TGA and DTG curves, appears at 60 ºC for 4% trapped water mass loss. Also in accordance with Raman results (50% sp3 sites), and a greater amorphous carbon content, one can see a greater 16% mass loss before CNT decomposition temperature. Although the most striking evidence of functionalization is shown by the 410 ºC CNT decomposition temperature. This 110 ºC temperature shift, in comparison with pristine sample, supports a weakened sp2 framework for CNT. The remaining 7% mass can be attributed to the catalysts metallic particles leftover.

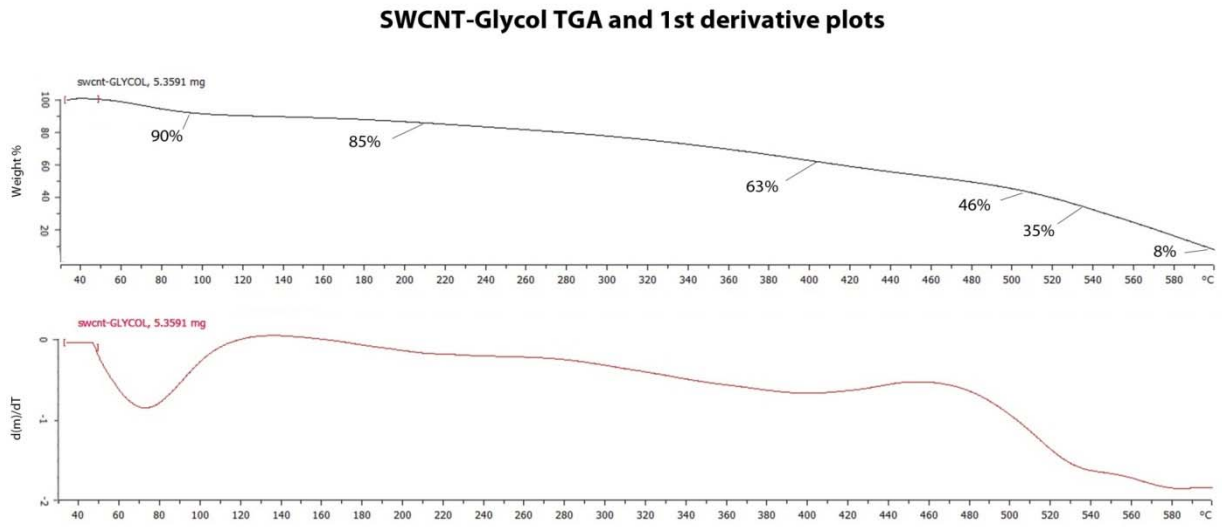

Figure 33. Thermal gravimetric analysis and DTG plots of SWCNT-Glycol molecule

The SWCNT-Glycol curve as can be seen is very different from the previous SWCNT plots. The initial 10% mass loss peak seems to be shifted about 10 ºC, as shown very clearly in the DTG curve, this can be attributed to a greater interaction of water with the glycol chains. As shown in Raman results (27.8% sp3 sites), this sample experience 27% mass loss before reaching CNT decomposition temperature. This unusual mass loss is due to the fact that the functional polyethylene glycol groups increase molecular weight significantly. Although Raman shows this has the greatest amorphous carbon content is not possible to determine it with the TGA or DTG plots since it overlaps with PEG peaks. Still one can actually see a peak 5% mass loss at 220ºC, which is close to the PEG200 boiling point. The next peak at 400 ºC can come from longest PEG chains. The decomposition temperature in this sample is 460 ºC that compared with SWCNT-COOH (410 ºC/50% sp3 sites), and pristine sample (520 ºC/5.7% sp3 sites) reveals intermediate weakening of sp2 framework.

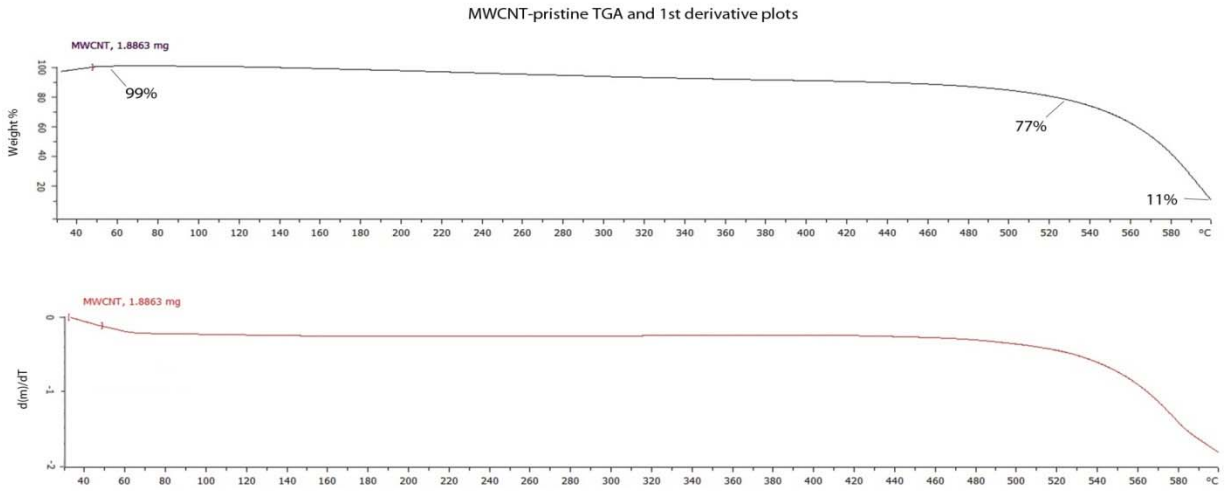

Figure 34. Thermal gravimetric analysis and DTG plots of MWCNT-pristine molecule

The pristine MWCNT sample shows a 1% mass loss immediately at 60 ºC that becomes much more apparent in the DTG curve. The IR shows little carboxylic acid functionalization and the Raman shows great number of defect sites. Nonetheless, one must keep in mind that core CNTs are shielded from the effects of Raman and as such no dipole moments are produced for core tubes giving an off reading. In fact the TGA shows an increase in CNT decomposition temperature of 530 ºC, regarding the large presence of defect sites. Then you can observe a leftover 11% mass corresponding to the metallic particles leftover.

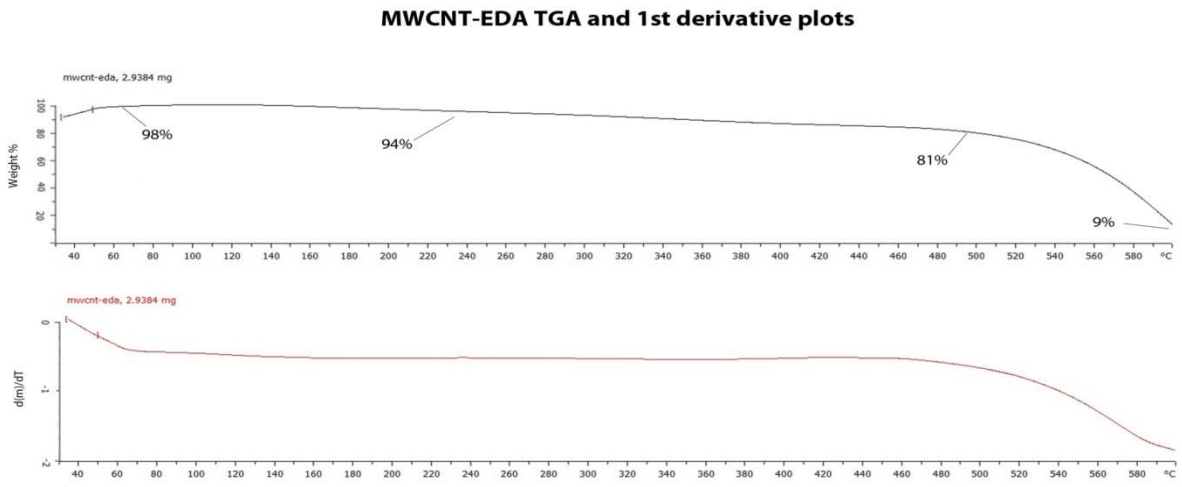

Figure 35. Thermal gravimetric analysis and DTG plots of MWCNT-EDA molecule

The MWCNT-EDA curve shows an increase in water content of 1%, which would correlate with the presence of hydrophilic groups in the surface. Although mass loss of the ethyelendiamine groups is expected at 200 ºC, no perceivable peak is found in either TGA or DTG curves. Infrared does confirm the presence of amine groups, although the absence of a peak in the TGA/DTG may be explained by the low 10% functionalization shown in the Raman spectrum. One can also observe that there is no distinguishable shift in decomposition temperature. This phenomenon can easily be explained by taking notice that even though the external CNT sp2 framework is in fact weakened by functionalization, the internal tubes are not.

2.6.8 Nuclear Magnetic Resonance of SWCNT-GLYCOL

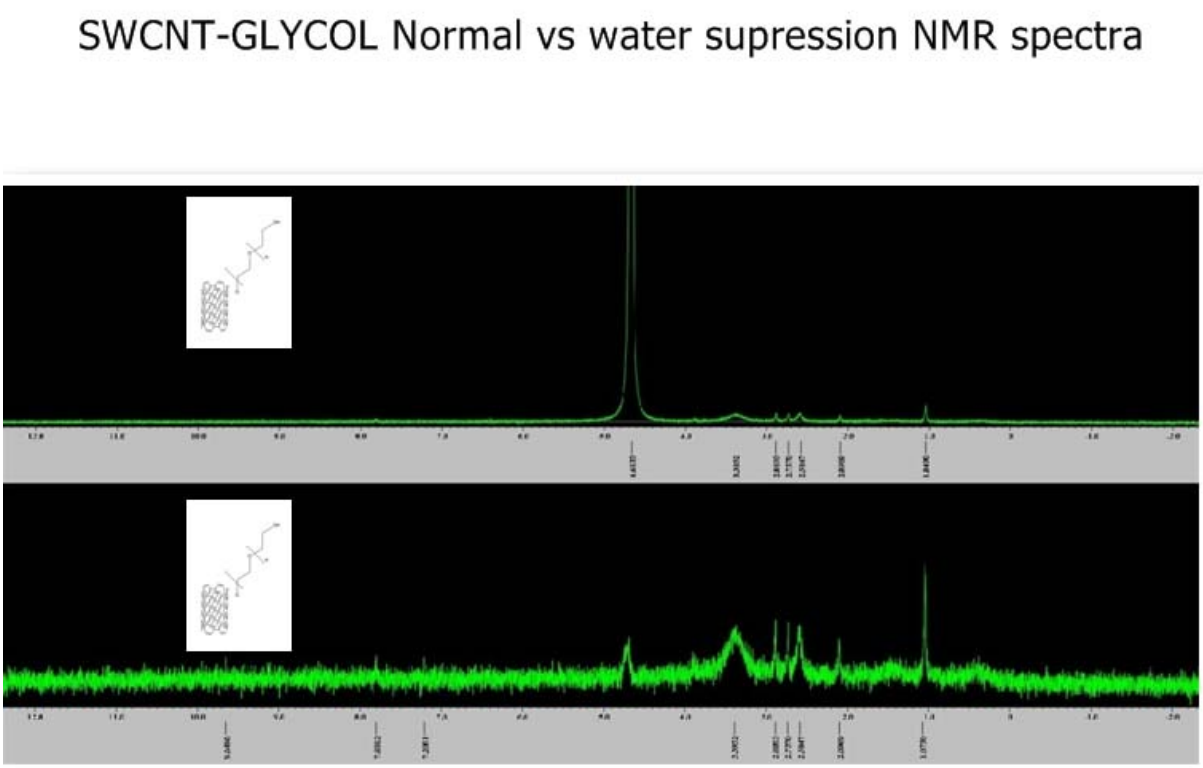

Figure 36. HNMR spectrum of SWCNT-Glycol sample

All functionalized single-wall and multi-wall carbon nanotube suspensions were scanned for NMR spectra. As shown in the solubility section of this thesis, one can see that the most stable CNT suspension was the SWCNT-Glycol, followed by SWCNT-COOH, and finally MWCNT-EDA. The two later suspensions didn't yield and NMR spectra most likely because of shimming problem due to large particles in solution. Separation of large particles through filtration and centrifugation still yielded no spectra. As such this is strong proof that the SWCNT-Glycol is the most stable suspension and forms the smallest aggregates.

The intensity of NMR signals dependent on abundance, therefore it is to be expected that the functional groups that only cover partially the surface of the nanotubes yield small signals. This coupled with the fact that the sample is soluble in water (huge signal), leaves barely

distinguishable absorption peaks. Nonetheless, through water suppression one can increase the signals as seen in the above figure. The signal at 1.2 ppm comes from the methylene protons, which might come from defect sites at the CNT. The D_2O water peak appear at 4.63 ppm and should appear at 4.78 ppm, therefore the peak is shifted downfield by 0.15 ppm. This shift confirms the presence of methylene either from contaminants or defect sites. The spectra also suggests, due to the signals thickness, some sort of glycol chain folding as expected. The cluster peaks between the methylene and the D_2O peak are from methylene in the polyether chain. Due to the asymmetry on the molecule the methylene signals break into several peaks with the widest peak at 3.4ppm corresponding to the methylene in the middle of the glycol chains. The up-field peaks around 2.7 ppm corresponds to the methylene close to the alcohol or the CNT end. Most likely the absence of the alcohol protons is due to deuterium displacement due to the abundant D_2O.

2.6.9 Confocal microscopy

Spectroscopic evidence provided important information for the selection of an ideal candidate for gene detection. Even though, photographic evidence is of the uttermost importance to show CNT/DNA interactions, and observe sequence specific aggregation. Confocal microscopy was used in order to demonstrate the interaction between CNT and DNA.

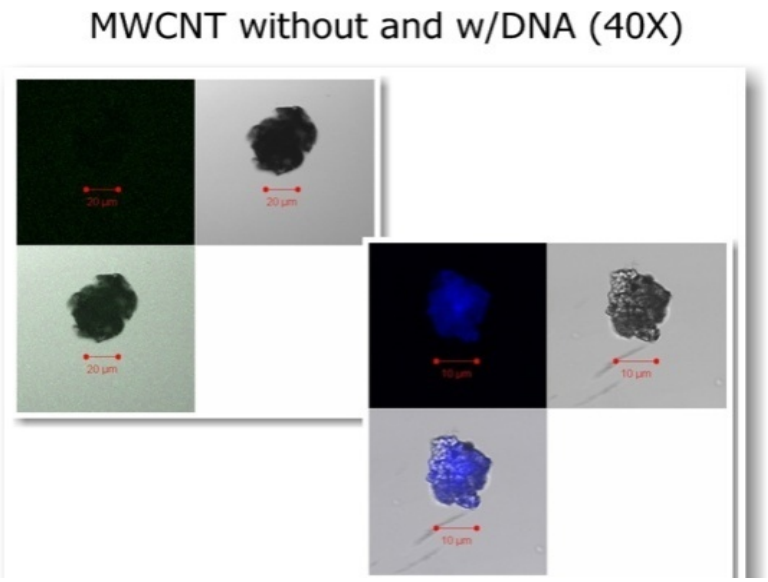

Figure 37. Confocal microscope pictures of pristine multi-wall samples and CNT/DNA complex suspensions. The picture on the left id bright field and the one on the right is using the UV for DAPI excitation.

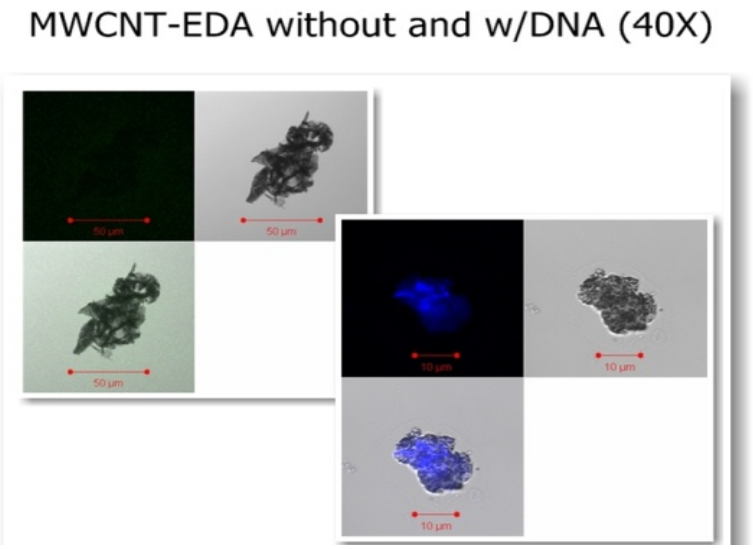

Figure 38. Confocal microscope pictures of pristine MWCNT-EDA samples and nanotube/DNA complex suspensions. The picture on the left id bright field and the one on the right is using the UV for DAPI excitation.

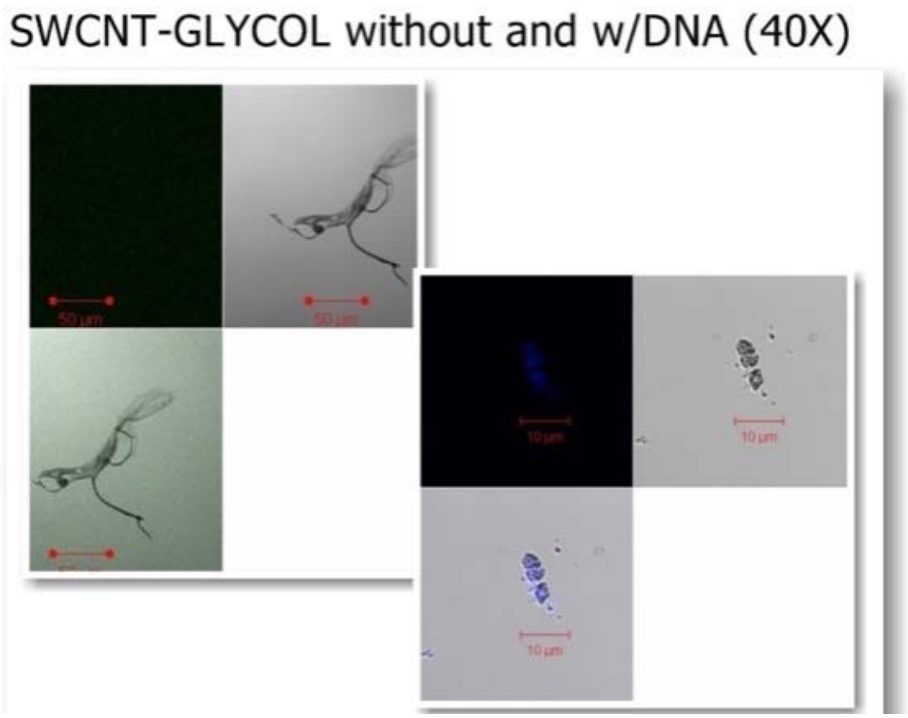

Figure 39. Confocal microscope pictures of pristine SWCNT-GLYCOL samples and nanotube/DNA complex suspensions. The picture on the left id bright field and the one on the right is using the UV for DAPI excitation.

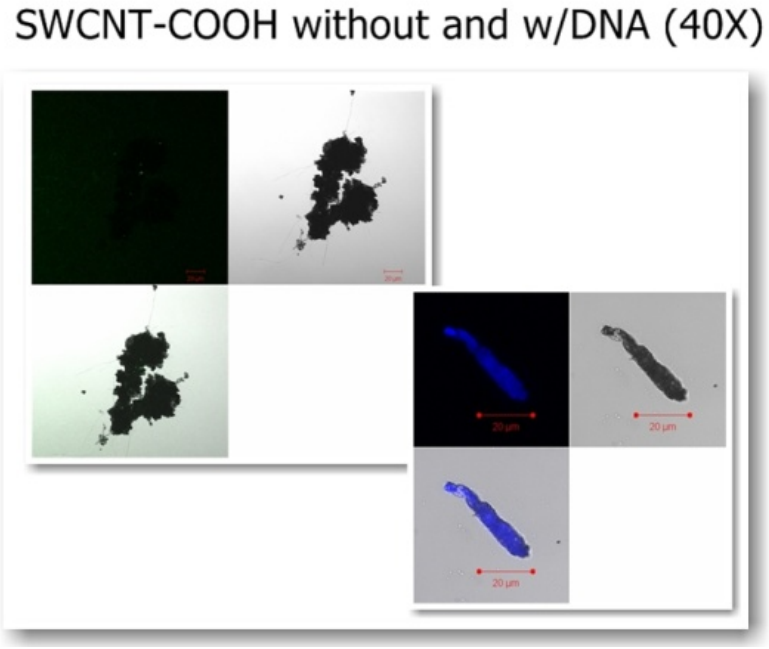

Figure 40. Confocal microscope pictures of pristine multi-wall samples and CNT/DNA complex suspensions. The picture on the left id bright field and the one on the right is using the UV for DAPI excitation.

All CNTs photographs are for very large aggregates found in the slide. In the dark field pictures, on the left, you can observe CNT bundles that don't fluoresce when subjected to excitation wavelength of DAPI DNA dye (450 nm). The photographs on the right show a CNT aggregate that seems to be covered in with something that reflect light in a different matter. The dark field photograph reveals the presence of DNA.

Analysis of the dark field aggregates without DNA for the different CNT samples reveal different aggregate behavior.

In the case of the MWCNT-EDA you can observe a more relaxed structure in comparison with the MWCNT. This most likely is due to the decreased association between CNTs because of the surface molecules. The SWCNT-Glycol sample was very hard to find a large aggregate and it seems looks with very low density. The SWCNT-COOH sample shows a very compact large bundle. These observations coincide with suspension stability observation for MWCNT and SWCNTs. Finally, the CNT aggregates seem to decrease in size with DNA addition.

In order to detect aggregation with Dynamic Light Scattering, for which the detection limit is 10 μm, a CNT sample that form stable suspensions with no bundles is essential. As such, the fact that DNA helps to increases the suspension qualities is very helpful. The fact that large aggregates are observed in the microscope is evidence that CNT sample centrifugation is key before DNA introduction.

2.6.10 Scanning Electron Microscope (SEM) of CNT samples

In order to confirm information gathered from the confocal microscope, SEM micrographs were acquired without DNA. To study the aggregates at a closer range photos were taken at low resolution (up), and compared to high resolution (down). Just as well EDAX analysis was conducted for all the CNTs.

MWCNT SEM AND EDAX

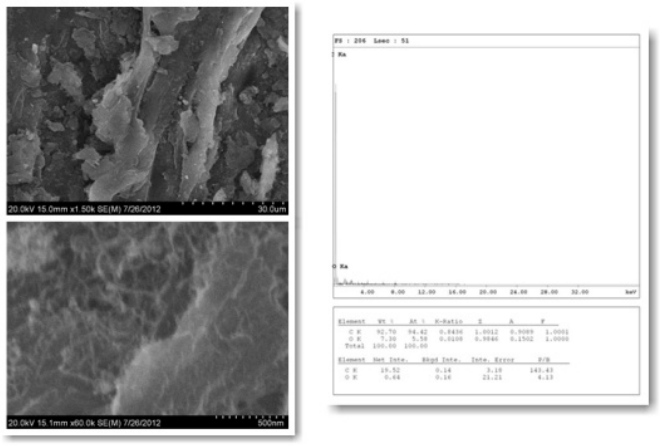

Figure 41.SEM pictures of pristine multi-wall carbon nanotube. The pictures on the left are different magnifications of the CNT samples and the picture in the right is the elemental analysis of the same sample

MWCNT-EDA SEM AND EDAX

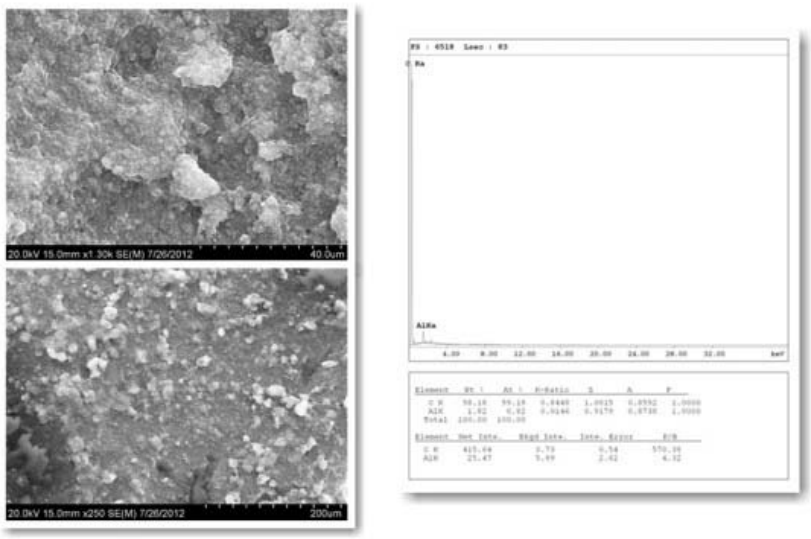

Figure 42. SEM pictures of pristine MWCNT-EDA carbon nanotube. The pictures on the left are different magnifications of the CNT samples and the picture in the right is the elemental analysis of the same sample

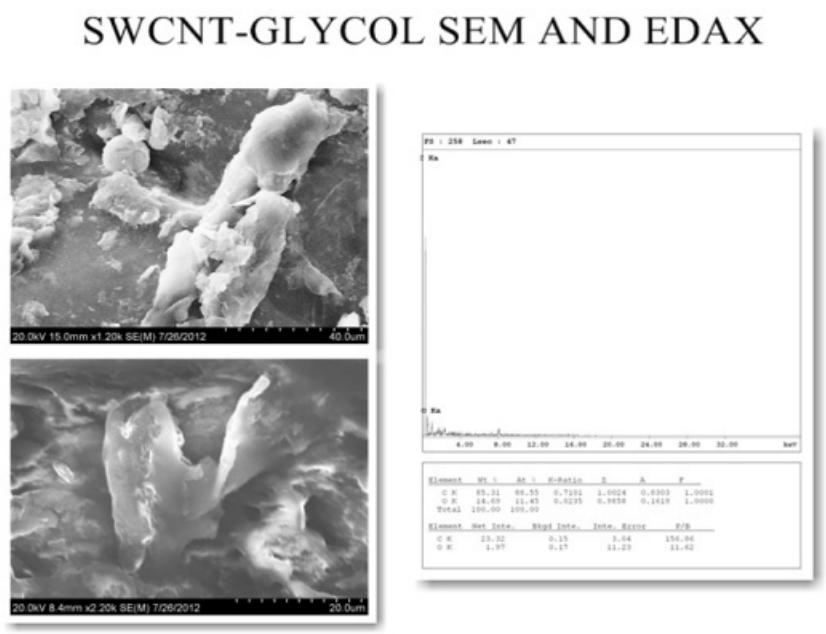

Figure 43.SEM pictures of pristine SWCNT-GLYCOL carbon nanotube. The pictures on the left are different magnifications of the CNT samples and the picture in the right is the elemental analysis of the same sample

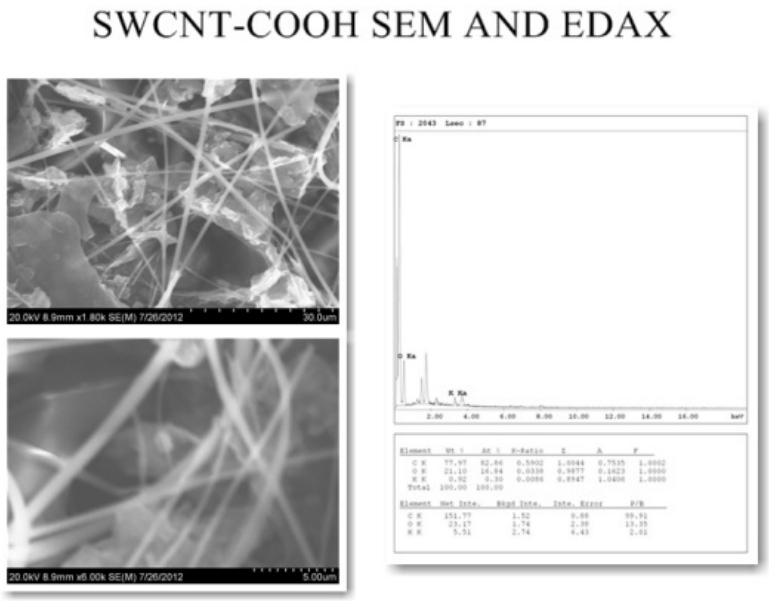

Figure 44.SEM pictures of pristine SWCNT-COOH carbon nanotube. The pictures on the left are different magnifications of the CNT samples and the picture in the right is the elemental analysis of the same sample

These are SEM pictures along with the elemental analysis of each one. As one can see the pristine MWCNT sample forms more even aggregates due to their high interaction forces. On the other hand the MWCNT-EDA seems to form more disperse aggregates. The SWCNT-GLYCOL picture on the other hand seems to aggregate as well when the water medium is removed, which came as a surprise. Finally it seems that without water the carboxylated CNTs form the least bundled of all of the samples. Although as one can observe from the light microscopy photos the SWCNT-COOH sample had little hairs sticking out (non-aggregating CNTs), the best candidate after careful analysis was the SWCNT-GLYCOL sample for DLS analysis.

Although as observed in all of the previous micrographs water is too polar of a medium for good suspensions of CNTs. As such a mixture of isopropanol and water by 50% volume was used for the aggregation experiments.

2.6.11 Raman spectroscopy for DNA interaction

To determine the interaction between CNT and the oligonucleotide 1 sequence with spectroscopy, Raman technique showed to display the most obvious signal shifts, and illustrated the best the type of interaction between these two molecules.

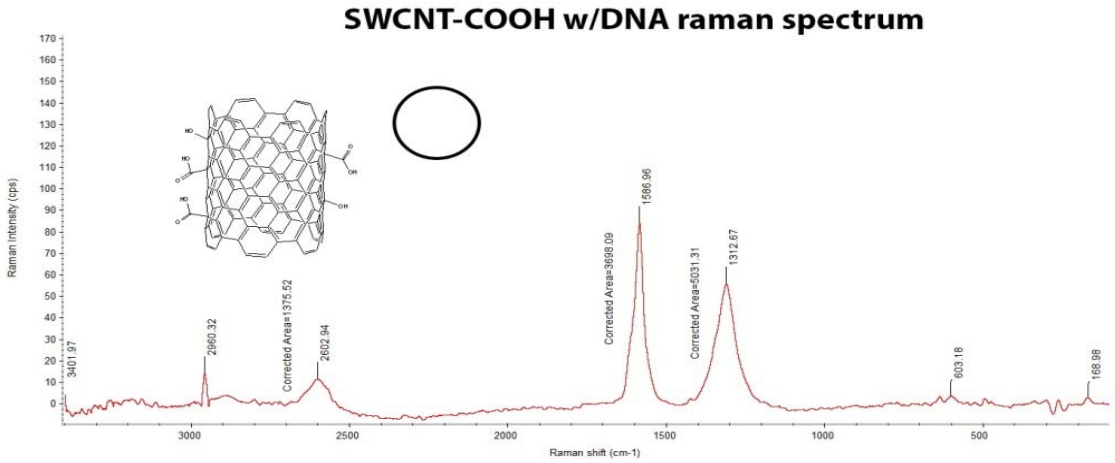

Figure 45. Raman spectra of SWCNT-COOH sample with oligonucleotide

The SWCNT-COOH with DNA spectrum shows that the G-band located at 1586.96 cm^{-1}, and a D-band at 1312.67 cm^{-1}. The intensities for the bands are 54.15 cps and 84.21cps, respectively. As such, the I_D/I_G = 0.643 showing a shift from the 0.5044 ratio of SWCNT-COOH sample, which makes sense if DNA is binding free sp2 sites, and as such decreasing the ratio of the intensities. Interaction with DNA is supported by the 8.46 cm^{-1} shift in the G-band that results in higher energy needed for stretching of sp2 sites. Finally, the most revealing evidence for loading of DNA lies in the disappearance of the RBM peaks at 260.15 and 162.13cm^{-1}. Then you can also observe a G' band shift of 24.7 cm^{-1}

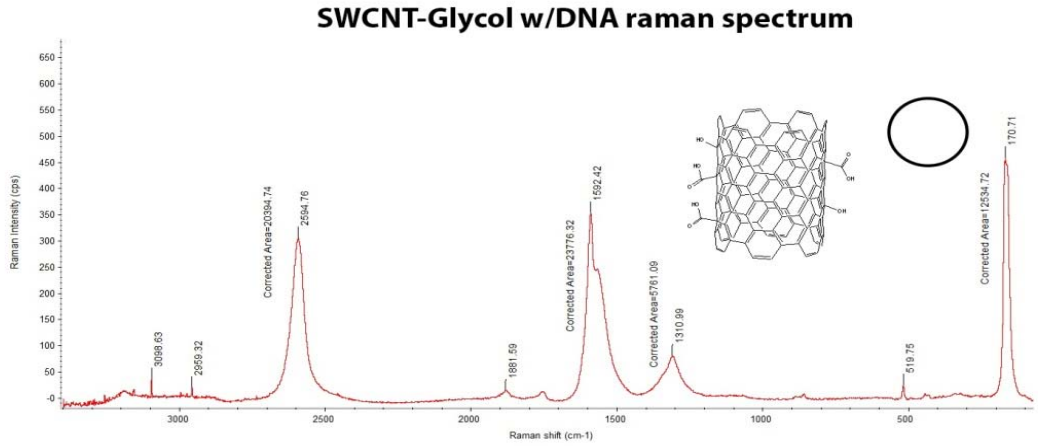

Figure 46. Raman spectra of SWCNT-Glycol sample with oligonucleotide

The SWCNT-Glycol with DNA spectrum shows that the G-band located at 1592.42 cm^{-1}, and a D-band at 1310.99 cm^{-1}. The intensities for the bands are 141.93 cps and 481.47cps, respectively. As such, the I_D/I_G = 0.194 showing a shift from the 0.335 ratio of SWCNT-glycol sample, showing the same behavior as the previous sample of DNA binding free sp2 sites. Again this sample also loses one RMB peaks at 519.75cm^{-1}, and the one at 170.71 cm^{-1} shows decrease intensity. Then you can also observe a G' band shift of 9.76 cm^{-1}. Finally in this sample, shows a change in the Breit–Wigner–Fano region of the G-band from having three shoulders in the

SWCNT-glycol sample to having two in this spectrum, which gives further evidence of DNA interaction (46).

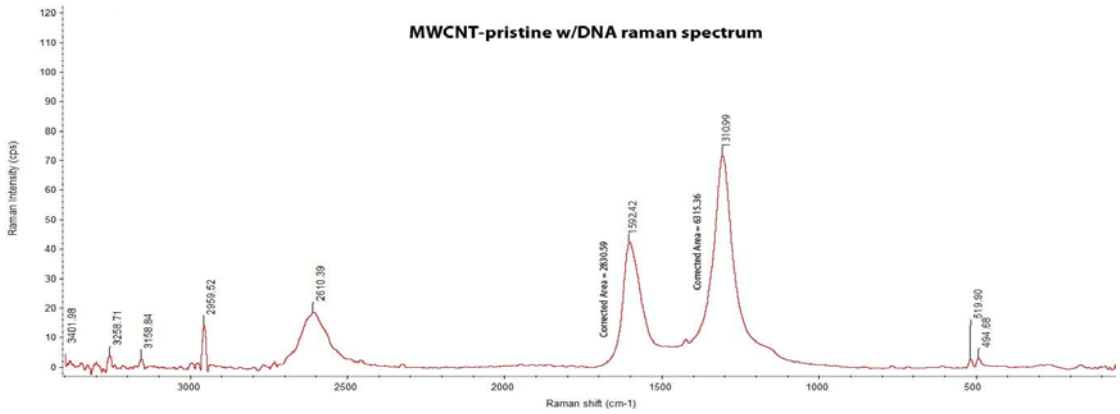

Figure 47. Raman spectra of MWCNT-pristine sample with oligonucleotide

The MWCNT with DNA spectrum shows that the G-band located at 1592.59 cm^{-1}, and a D-band at 1310.99 cm^{-1}. The intensities for the bands are 59.45 cps and 34.54cps, respectively. As such, the I_D/I_G = 1.70 showing a shift from the 1.68 ratio of MWCNT sample. Interaction with DNA is supported by the large 12.95 cm^{-1} shift in the G-band that results in higher energy needed for stretching of sp2 sites. You can also observe a decrease in the intensity of the peak found, at 519.90 $^{cm-1}$, also no G' band shift.

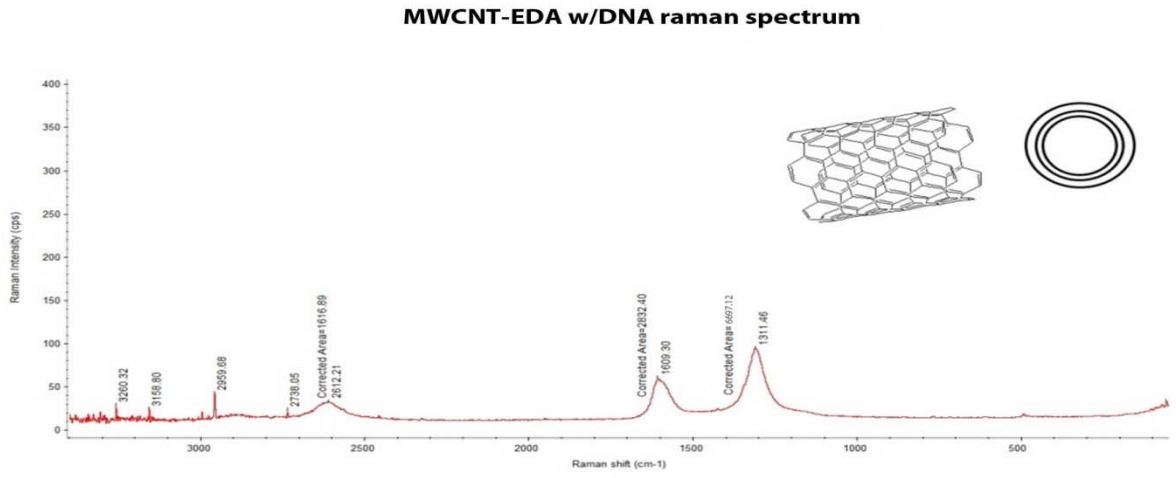

Figure 48. Raman spectra of MWCNT-EDA sample with oligonucleotide

The MWCNT-EDA with DNA spectrum shows that the G-band located at 1609.30 cm^{-1}, and a D-band at 1311.46 cm^{-1}. The intensities for the bands are 65.37 cps and 38.74cps, respectively. As such, the I_D/I_G = 1.97 showing a shift from the 1.84 ratio of MWCNT sample, which is the most significant evidence in this sample of DNA interaction through sp2 hindering. Finally there is also a 1.88 cm^{-1} G' band shift.

CHAPTER 3

3.1 Dynamic Light Scattering (DLS)

Spectroscopic and microscopy characterization of f-CNTs/CNTs determined that the SWCNT-Glycol sample was the most appropriate for aggregate candidate for aggregate formation. Evidence demonstrated the sample was superior in terms of suspension stability, nanotube integrity, and showed it didn't tend to form large aggregates. DLS was conducted to determine if this event could be detected for easier clinical detection of any gene. This is a very complicate technique that requires immaculate sample preparation. Any dust particle contaminant, bubble, or source of nuclease contamination could impair the experiment. Therefore, treatment of water and its loading into measuring cell was as important as CNT sample preparation. Further experiments were conducted to determine if known hybridization buffers like saline-sodium citrate (SSC) would aid in hybridization. CNT-Glycol concentration was also a concern, as such experiments were conducted for parameter determination, and finally incubation time was also followed.

3.1.1 Water treatment

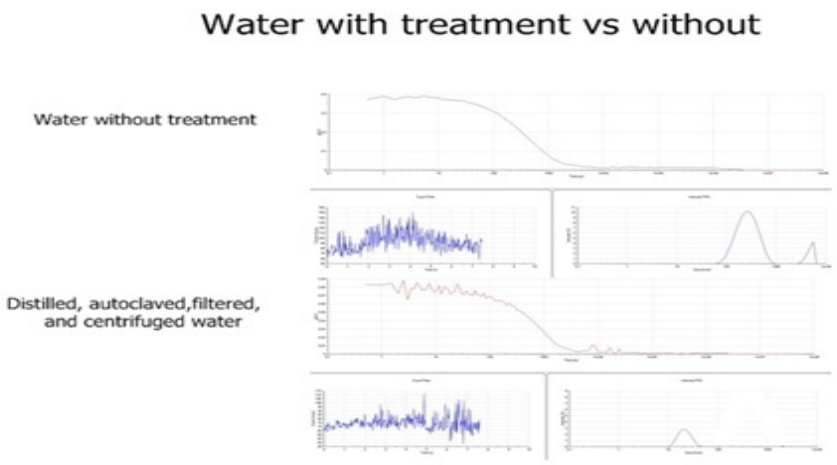

Figure 49.Dynamic light scattering spectrograms of water used in experiments before and after treatment

Thorough treatment of the water used for the preparation of the samples was carried out to remove completely of DNAses and dust particles. Water was collected from milliQ filtration systems and distilled on thoroughly rinsed glassware in an attempt to isolate the condensed water from the dust in the air. Later the water was filtrated, and collected in clean glass bottles, followed by vacuum degasing. The final step before storing involved the autoclaving of the water filled bottles to denature any remainder DNAses. Before using the water, the desired volume was removed in a hood and transferred to Eppedorf tubes for centrifuging at 6000 R.P.M for thirty minutes. In this case the measurement yielded the riddance of some bigger dust particles that would introduce a lot of noise in the system otherwise.

3.1.2 Concentration

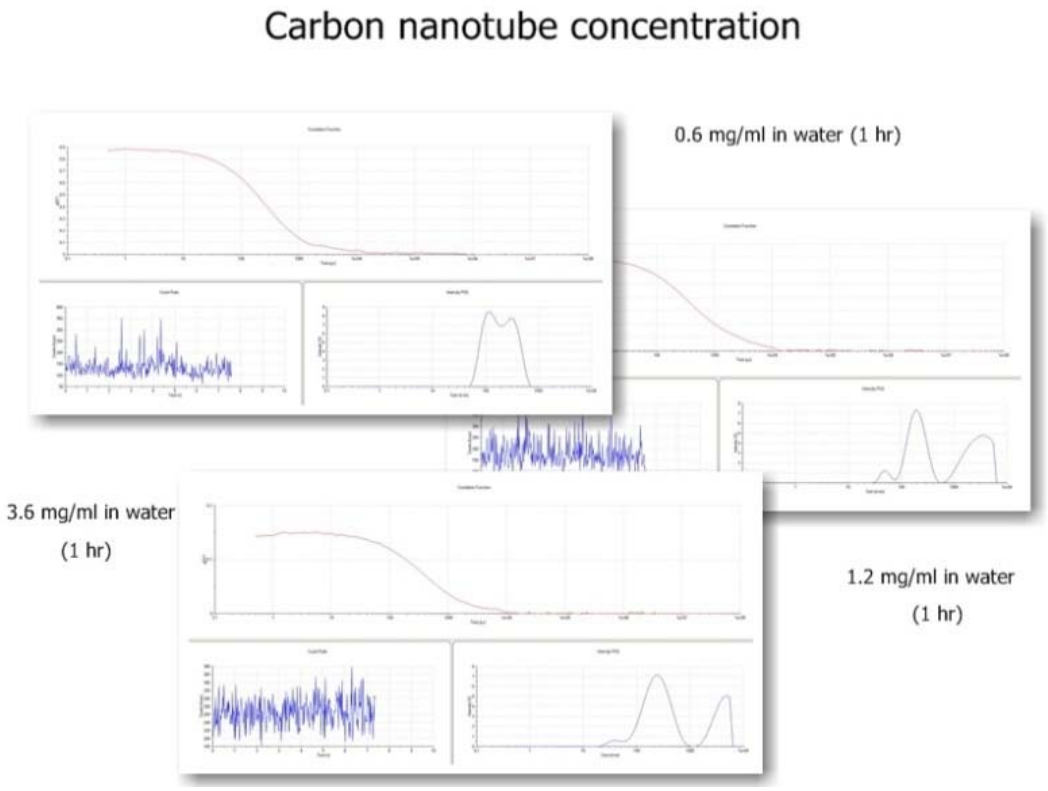

Figure 50. Dynamic light scattering spectrograms of SWCNT-GLYCOL at different concentrations

In order to determine the effect of concentration on the DLS spectra three solutions with different CNT concentrations were subjected to analysis. The chosen concentrations were based

on the solubility of the CNTs sample and the visual optical density of the solution. In order not determine the concentration ranges that would allow light to reach the analyzer without problems and provide an intense signal 0.6, 1.2, and 3.6 mg/ml solutions were tested. Measurements show the concentrations above the commonly used, 0.5 mg/ml total, increases the aggregation behavior of the samples. The highest concentration graph on the farthest left of the picture (3.6 mg/ml) visually was shown to have precipitate. The highest concentration graph shows a peak at 100 nm and the other at 500 nm, although the DLS graph doesn't show those big aggregates that formed; as they go beyond the 10 um limit detection. Both the 1.2 mg/ml and the 0.6 mg/ml DLS plots show very similar behavior. Nonetheless, the graphs show start to show 10 um, which confirms decrease in aggregate size dependent on CNT concentration. Since the concentration at 0.6 mg/ml shows to generate smaller aggregates, in comparison in 1.2 mg/ml population peak shift, this was chosen as the ideal concentration for CNT detection.

3.1.3 Ionic strength

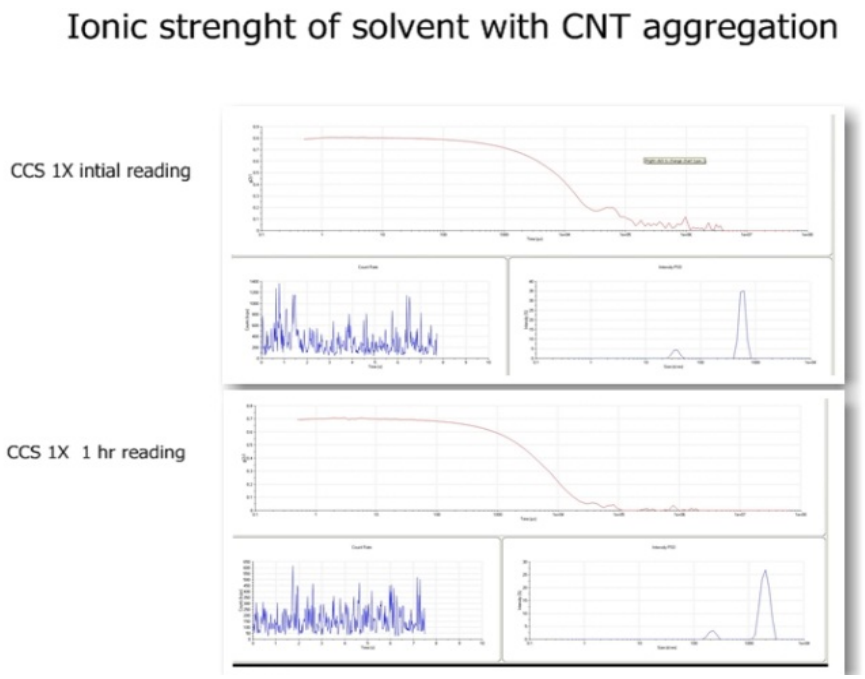

Figure 51. Dynamic light scattering spectrograms of SWCNT-GLYCOL with 1X SSC buffer

In experiments of DNA hybridization the buffer SSC is widely used to increase base pair recognition. As the project involves aggregation through sequence hybridization, it's essential to test the effect of ionic strength in the CNT suspensions stability. One can clearly see the increase in size of the CNTs. Since the logarithmic detection limit is 10 umm, there is an immediate CNT population shift from 200 nm maxima to 800 nm, so it narrows down the detection space for aggregation. There is an obvious repulsion of the CNTs from the medium, since after 1hr there is an increase in population size to a maximum of 2um. In fact, what is observed in the spectrum is only a part of what really happens, since the sample without DNA completely precipitated within seconds.

3.1.4 Molecular Ratio experiment

In order to observe sequence dependent aggregation is essential to compare with appropriate controls. In this case SWCNT-Glycol without DNA and SWCNT-Glycol with oligonucleotide 1 sequence only were used as controls. Molecular ratios of 1:1:1, 1:10:10, and 1:100:100 of CNT/Oligo1/Complementary oligo2 were chosen to refine aggregation conditions.

4.10.5 CNT-Glycol without DNA control

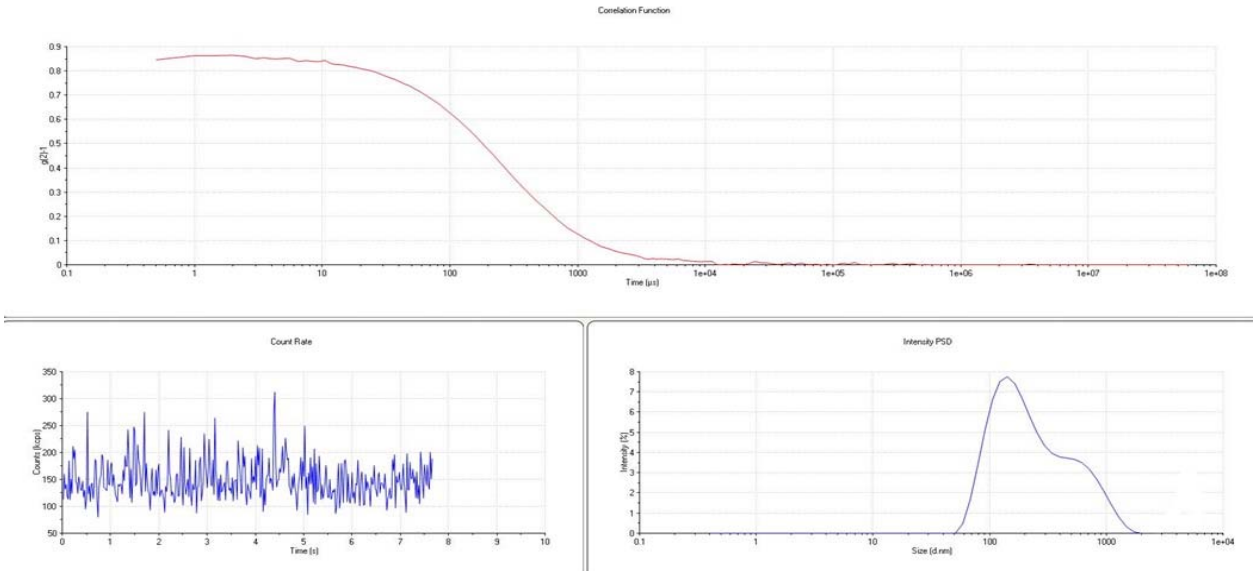

Figure 52. Dynamic light scattering spectrograms of SWCNT-GLYCOL control without DNA

This DLS graph corresponds to the water suspension of CNT-Glycol sonicated for 30 min. The peak in the size distribution shows a maximum at 100 nm, but also is very wide. This is most likely due to the wide size distribution of CNTs.

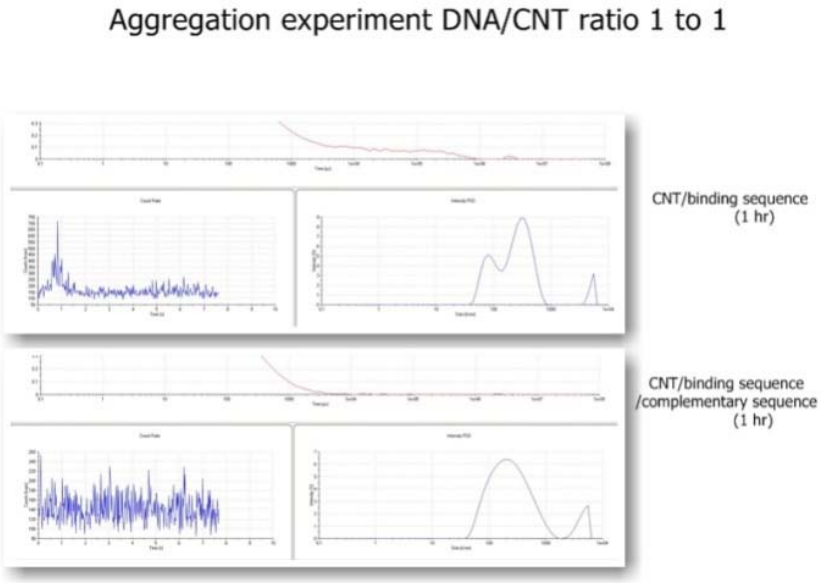

Figure 53.Dynamic light scattering spectrograms of SWCNT-GLYCOL with oligonucleotides one and two. Top spectrum is the mixture of the SWCNT-GLYCOL and the oligonucleotide one. The spectrum on the bottom is after addition of the second oligonucleotide; CND/DNA molecular ratio one to one

The picture above shows the population distribution for the CNT/Oligo1 on top, and the 1:1:1 ratio of CNT/Oligo1/Complementary Oligo 2 sample on the bottom. As observed there is no visible increase in size.

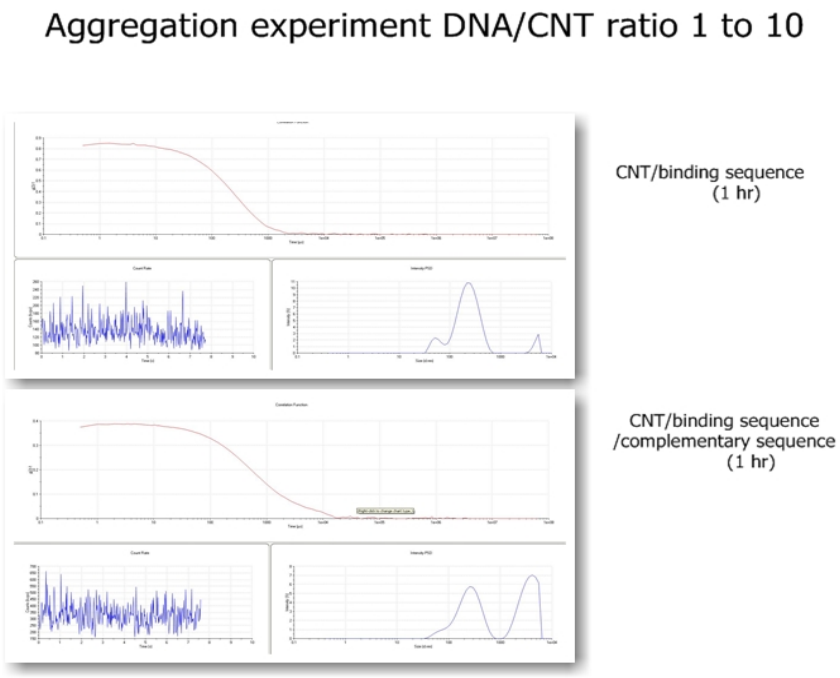

Figure 54.Dynamic light scattering spectrograms of SWCNT-GLYCOL with oligonucleotides one and two in a ratio 1:10

The picture above shows the population distribution for the CNT/Oligo1 on top, and the 1:10:10 ratio of CNT/Oligo1/Complementary Oligo 2 sample on the bottom. In picture you do see a radical increase in size, which compared to the CNT/oligo 1 sample, suggests sequence dependent aggregation.

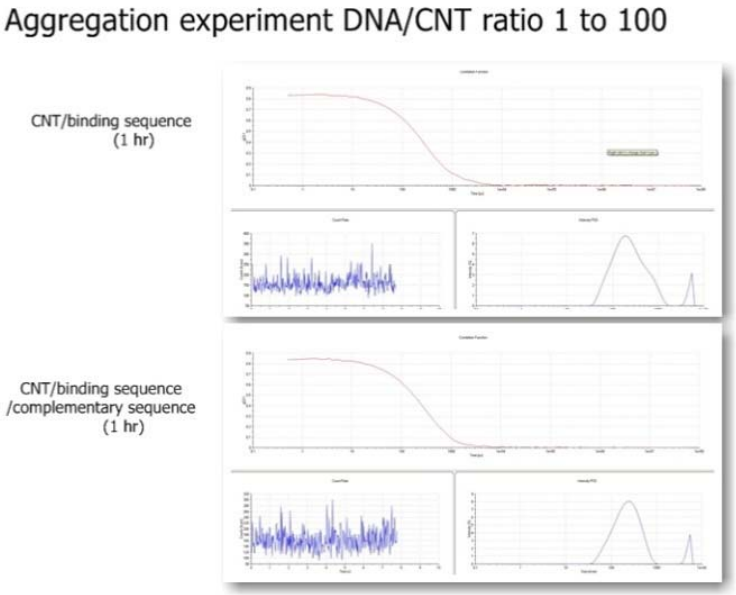

Figure 55.Dynamic light scattering spectrograms of SWCNT-GLYCOL with oligonucleotides one and two in a ratio 1:100

The picture above shows the population distribution for the CNT/Oligo1 on top, and the 1:100:100 ratio of CNT/Oligo1/Complementary Oligo 2 sample on the bottom. In picture you barely see an increment of size, which makes the ration 1:10:10 the most ideal for aggregate identification.

4.8 Studies with CNT samples and complementary oligonucleotides

3.2 Transmission Electron Microscope of chosen SWCNT-GLYCOL

So as to observe the aggregation behavior of SWCNT-Glycol upon the introduction of the complementary DNA sequences, TEM was explored. Since SWCNT-Glycol sample was considered to be the best, after all spectroscopic and photographic evidence, proper controls were used to confirm presence of sequence induced aggregation; pristine CNT, SWCNT-Glycol without DNA, and SWCNT-Glycol with oligonucleotide 1 only. Molecular ratios of 1:1:1, 1:10:10, and 1:100:100 of CNT/Oligo1/Complementary oligo2 were observed under the TEM microscope to assess the ideal conditions for aggregation.

The three molecular ratios were prepared with lots of care, in order to prevent nuclease, dust, and any type of artifact contamination. In order to prepare the 1:1:1 CNT/Oligo1/Complementary oligo2 sample, 3.73ug of oligo 2 and 2.80 ug of oligo 1, were mixed with CNTs in an isopropanol/nuclease-free water (50% v/v) solution with a final concentration of 5.44 ug/ml of DNA (0.76 nanomolar). The 1:10:10 CNT/Oligo1/Complementary oligo2 sample, contained 30.73 ug of oligo 2 and 20.80 ug of oligo 1, mixed with CNTs in an isopropanol/nuclease-free water (50% v/v), solution with a final concentration of 50.44 ug/ml of DNA (7.6 nanomolar). Finally, the 1:100:100 CNT/Oligo1/Complementary oligo2 sample, contained 300.73ug of oligo 2 and 200.80 ug of oligo 1, mixed with CNTs in an isopropanol/nuclease-free water (50% v/v), solution with a final concentration of 500.44 ug/ml of DNA (70.6 nanomolar).

Since current CNTs synthetic methods yield a wide variety of tube diameters, lengths, and in the case of SWCNTs all three conformations (Zig-Zag, Chiral, and Armchair), it is very difficult to calculate molar ratios from CNT weight. As such, a calculation was made to get the closest molar estimate possible. The average length value for SWCNT used was 1.5um and the average value for diameter was 0.6nm (57). Treating the CNT as a perfect cylinder a calculation was made to determine the area of an average CNT (565,468.87 A^2). This was then compared to the area that four planar benzenes would occupy (29.178 A^2) to acquire the average molecular weight of a SWCNT (3,724,172.96 g/mol). This approach determined the amount of CNTs required to meet the different CNT/Oligo1/Complementary oligo2 ratios.

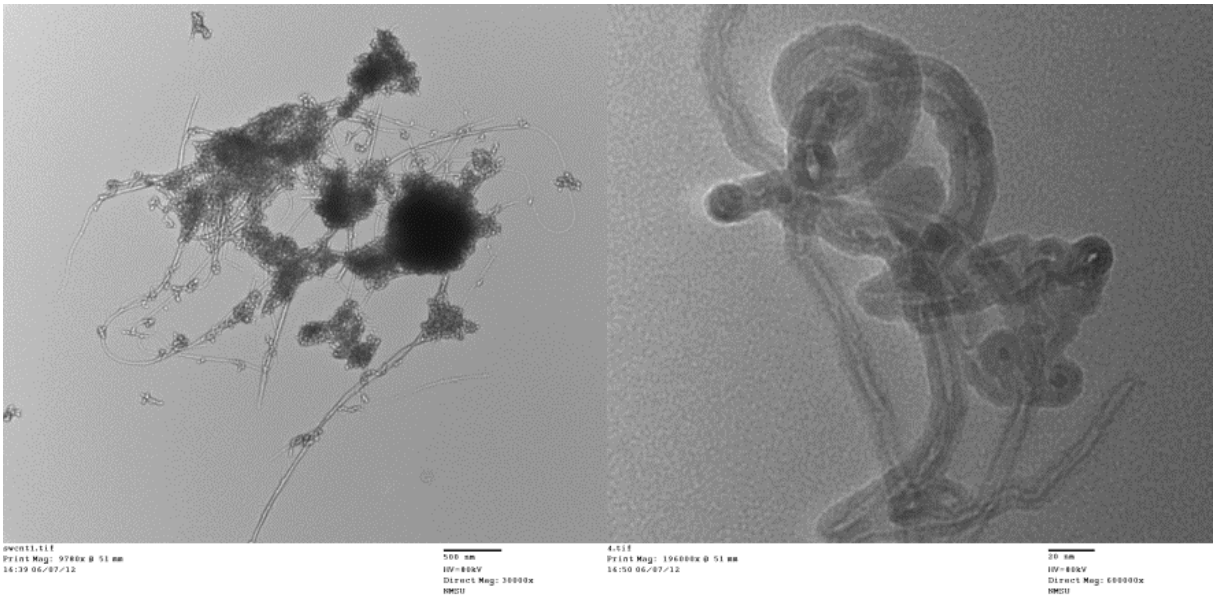

Figure 56. Transmission electron microscope pictures of pristine single-wall CNTs. The picture on the left is lower magnification than the one on the right.

Pristine SWCNT are not soluble in isopropanol/water, as such the stock had to be vigorously shaken before a droplet was loaded onto the Nickel grids. A small aggregate in the population was focused at 30,000X in the picture on the left. In here one can appreciate the dense entanglement that pristine sample achieves, as well as the presence or transparent metal catalysts.

The higher magnification photograph on the right, at 600,000X, shows the strong interactions arising between CNTs.

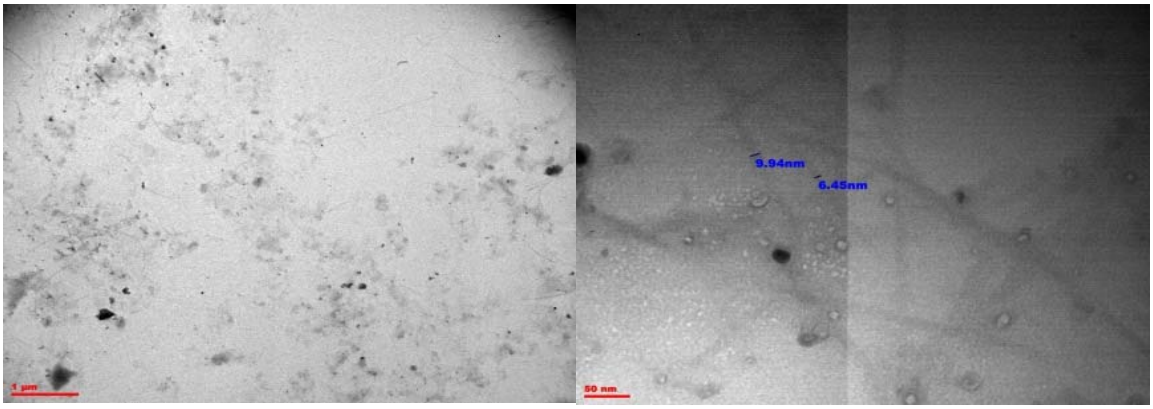

Figure 57. Transmission electron microscope pictures of SWCNT-glycol without DNA. The picture on the left is lower magnification than the one on the right.

Stable suspensions of SWCNT-Glycol seen in the microscope were completely dispersed by 30 min sonication, and supernatant collected after 6,000 RPM centrifugation for 30min. Controls of SWCNT-Glycol show that in contrast with SWCNT-pristine samples are much more spread. The picture on the left shows a low magnification picture of a field in which you can observe the presence of scattered SWCNT-Glycol, as well as amorphous carbon impurities. The picture on the right, at 200,000X, shows that the diameter of these scattered tubes is around 8 nm. The information acquired by the Raman shows that there are tubes of 0.5 and 1.6 nm, which would mean that the difference comes from the coating with the polyethylene glycol molecule.

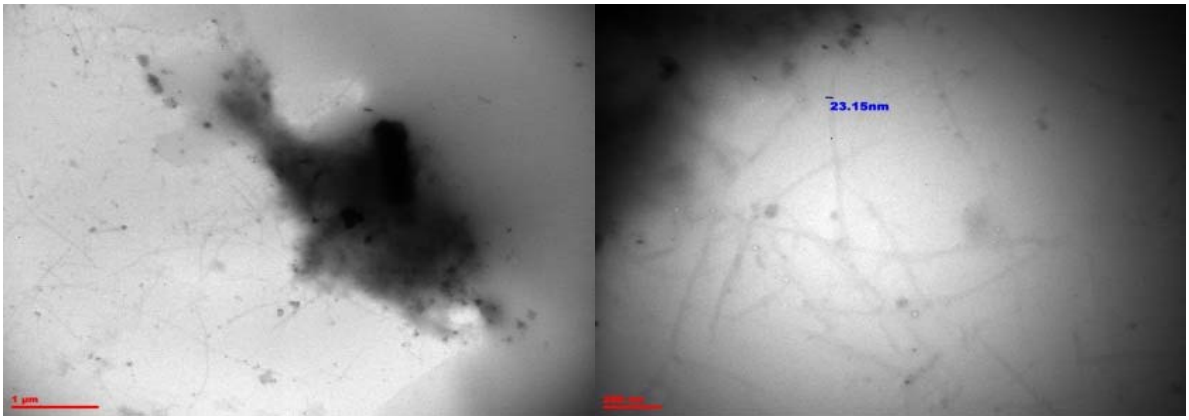

Figure 58. Transmission electron microscope pictures of SWCNT-glycol with oligonucleotide sequence 1.

Upon centrifugation the supernatant was collected and mixed in a 1:100 ratio of CNT/Oligo 1 control was observed under the microscope. Just as expected the pictures show a dispersed CNT sample in most regions observed. Among the regions scanned in the grid most contained unbound CNTs as seen in the CNT-glycol without DNA control, one artifact was found shown in the above pictures. The picture on the left shows this artifact, at 20,000X, that doesn't seem to be associated with the surrounding CNTs. In order to determine this, a picture was taken one the border of the artifact at a resolution of 63,000X, which in fact does confirm this as an artifact as no association is seen. The CNTs appear to have increased again in diameter (8 to 20 nm), which could arise from the coating of the CNTs with DNA.

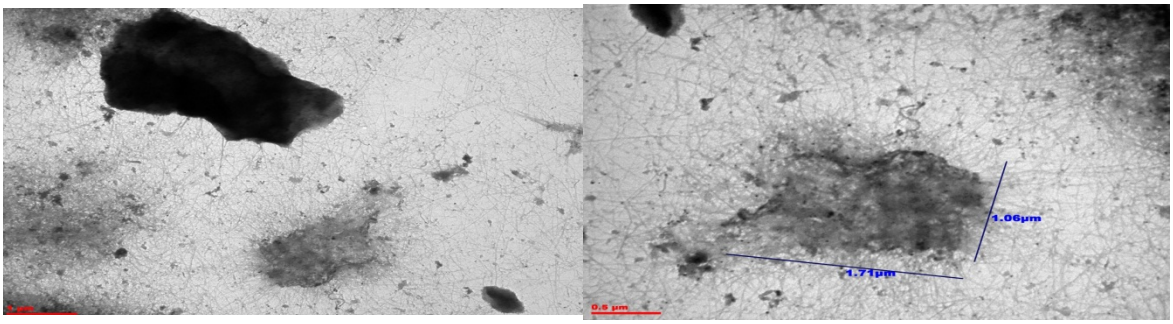

Figure 59. Transmission electron microscope pictures of SWCNT-glycol with oligonucleotide sequence 1, and complementary oligonucleotide 2 (ratio CNT/DNA of 1:1) The picture on the left is lower magnification than the one on the right.

Upon centrifugation the supernatant was mixed with DNA to achieve a 1:1:1 ratio of CNT/Oligo1/Complementary oligo 2, and was observed under the microscope. The picture on the left, at 16,000X, shows widespread aggregates which is consistent with bridging of CNTs through hybridization of complementary oligonucleotide sequences. The aggregates for the most part seem to be relaxed structures that decrease in density as you go farther away from the center. The picture on the right reveals that the dimensions of the aggregates are about 1 µm in length and width that reveals a couple of hundred nanotubes entangled for a CNT that tends to be spread in space.

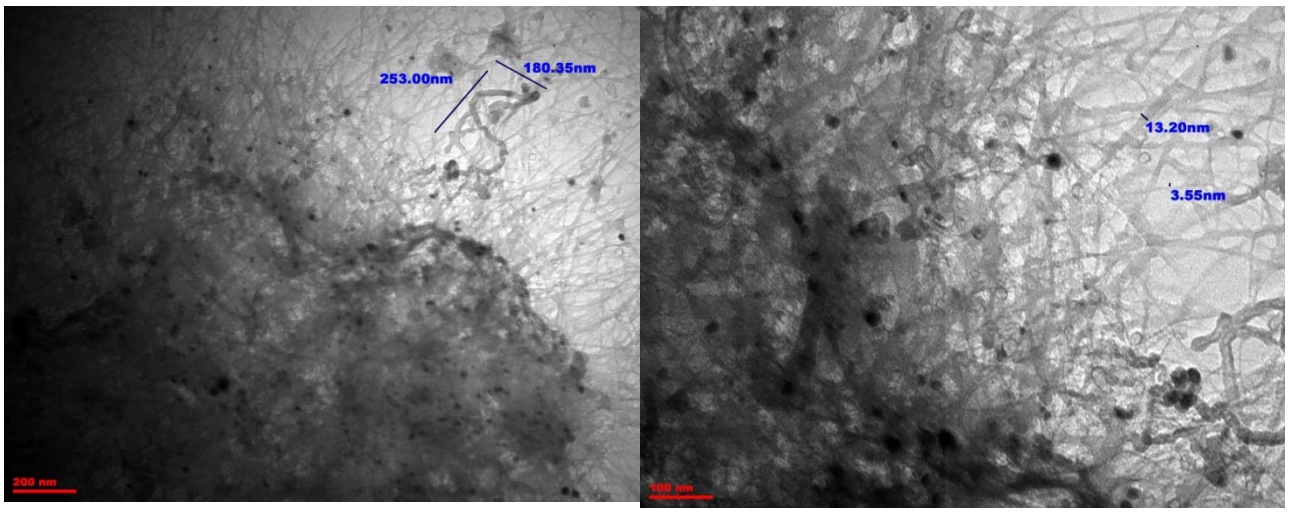

Figure 60. Higher magnification TEM pictures of SWCNT-glycol with oligonucleotide sequence 1, and complementary oligonucleotide 2 (ratio CNT/DNA of 1:1) The picture on the left is lower magnification than the one on the right.

The pictures on the top correspond to the same sample, but at higher magnifications; 63,000X and 125,000X. Both of these pictures are focusing on the edge of the aggregates to demonstrate associations with the surrounding CNTs with the center of the bundles. The density decrease as you leave the aggregate is strong evidence that this is in fact a CNT aggregate.

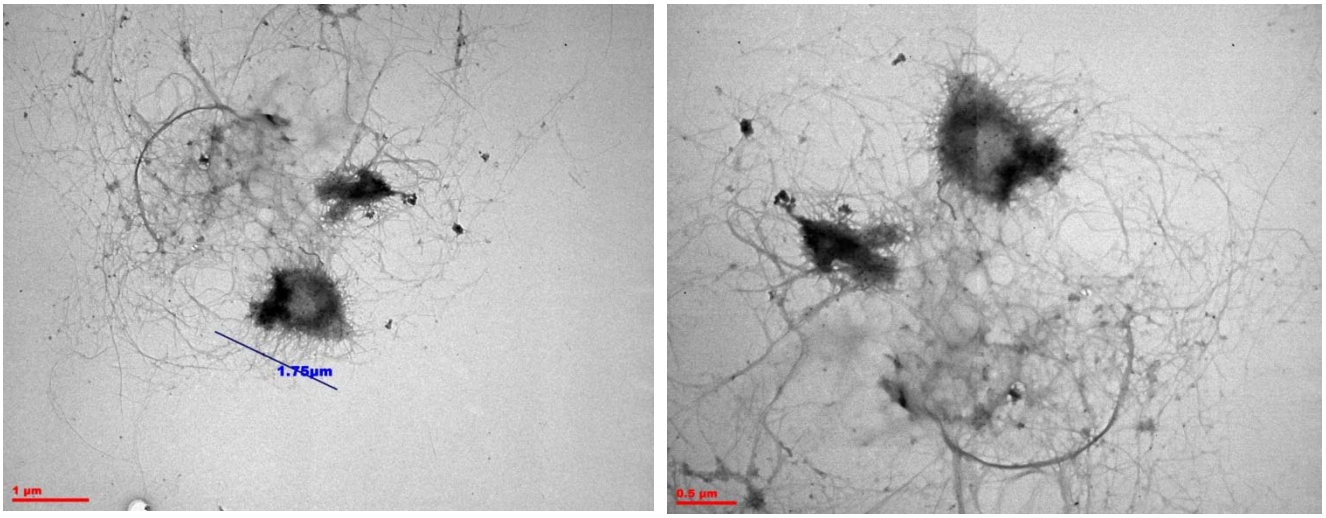

Figure 61. Transmission electron microscope pictures of SWCNT-glycol with oligonucleotide sequence 1, and complementary oligonucleotide 2 (ratio CNT/DNA of 1:10) The picture on the left is lower magnification than the one on the right.

Upon centrifugation the supernatant was mixed with DNA to achieve a 1:10:10 ratio of CNT/Oligo1/Complementary oligo 2, and was observed under the microscope. Both the picture on the left and right, at 16,000X and 25,000X, show the same type of aggregates as in the previous sample just a little bit larger. One can also observed that there are darker areas in the aggregates that can be attributed to higher density; as such it may be an indication that density is dependent on DNA content. The previous assumption makes sense if one thinks that CNTs can be bound at several places along its surface increasing contact with surrounding neighbors.

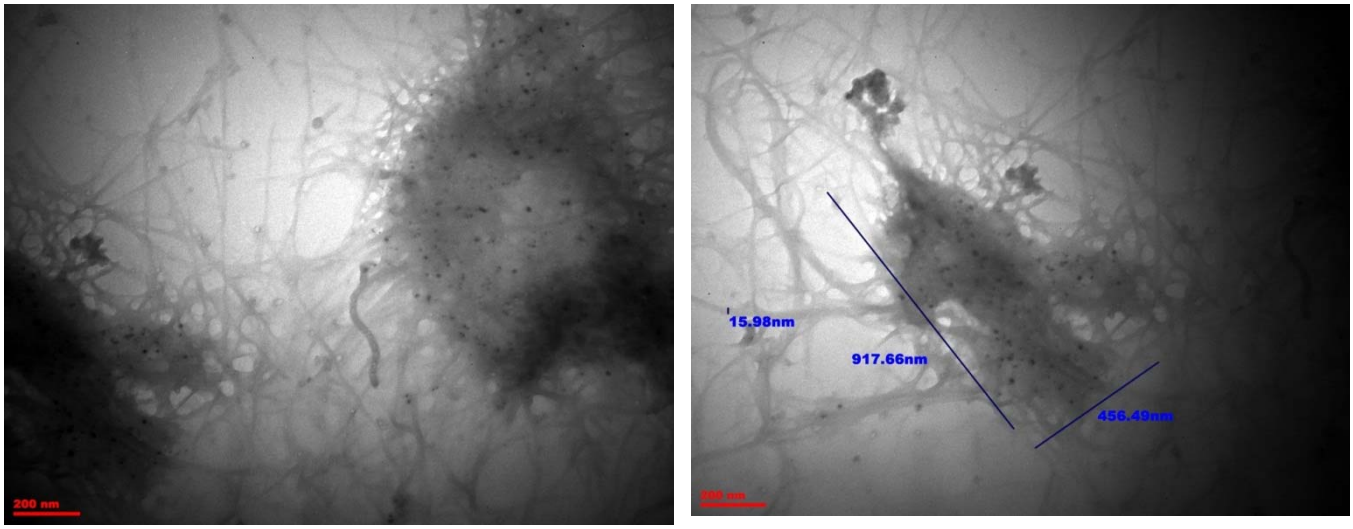

Figure 62. Higher magnification TEM pictures of SWCNT-glycol with oligonucleotide sequence 1, and complementary oligonucleotide 2 (ratio CNT/DNA of 1:10) The picture on the left is lower magnification than the one on the right.

The pictures on the top correspond to the same sample, but at higher 63,000X magnification. You can observe here as well an association between the surrounding nanotubes and the aggregate, and in here as well density seems to decrease as you leave the aggregate. It can be clearly observed that these materials can in fact work as gene sensors.

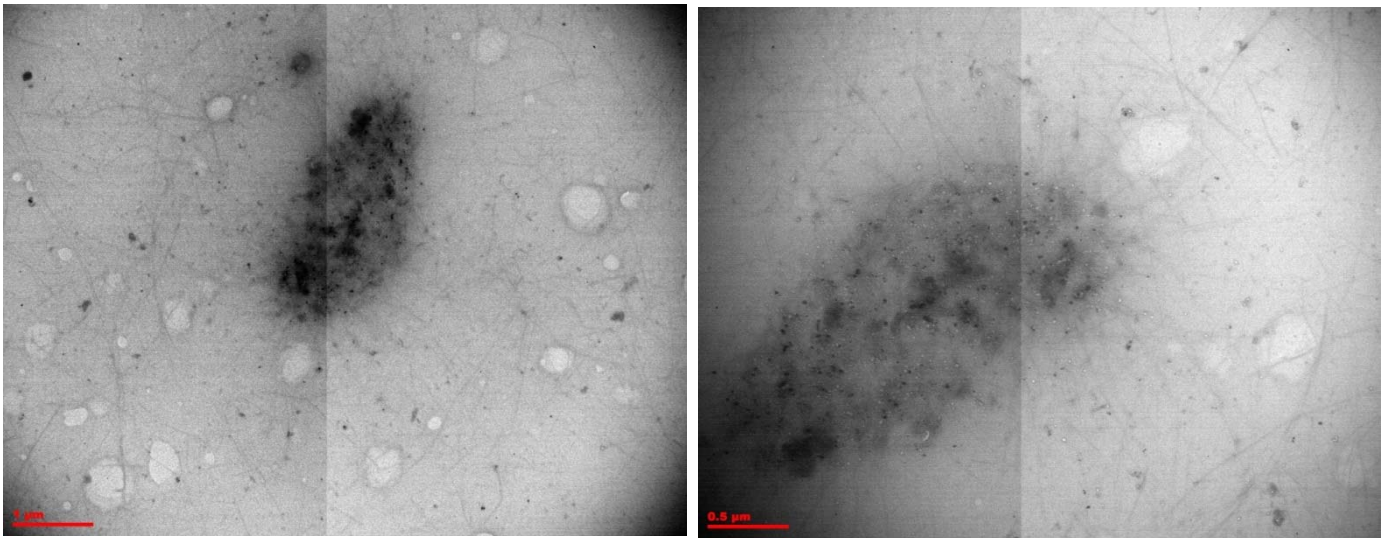

Figure 63. Transmission electron microscope pictures of SWCNT-glycol with oligonucleotide sequence 1, and complementary oligonucleotide 2 (ratio CNT/DNA of 1:100) The picture on the left is lower magnification than the one on the right.

Finally, the last sample of 1:100:100 ratio of CNT/Oligo1/Complementary Oligo 2 was observed under the microscope. Both the picture on the left and right, at 16,000X and 31,500X, one can observe an aggregate with the least density in all of ratio samples. This can be an indication of a saturation point of CNT-Glycol with DNA, a scenario in which available ends for hybridization are not as available as in the other ratios.

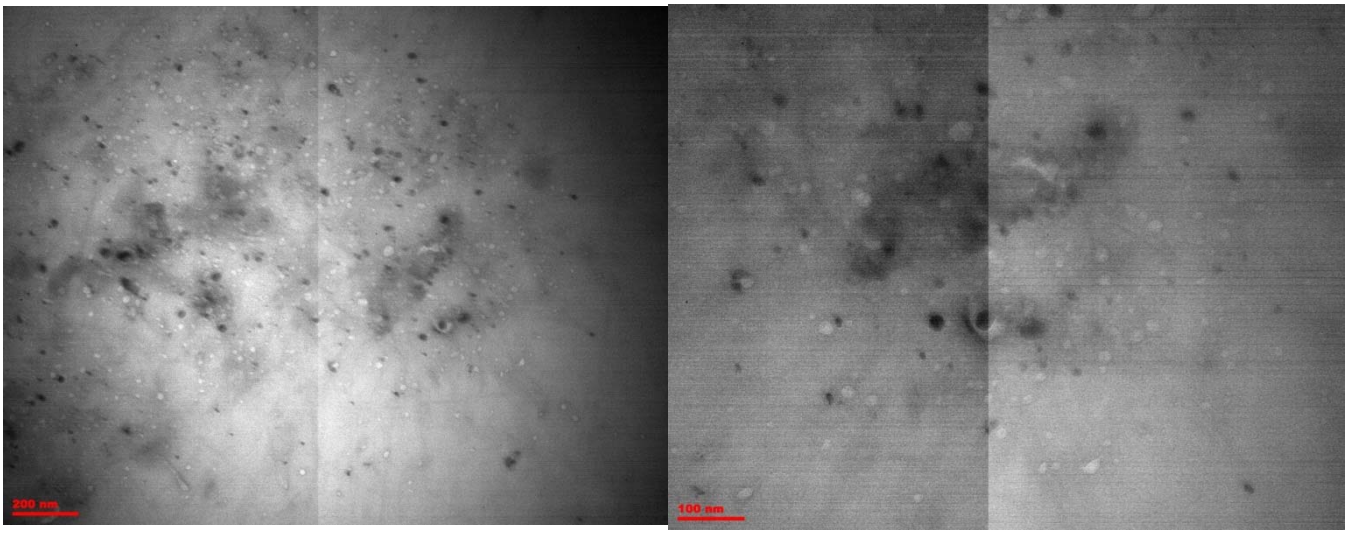

Figure 64. Higher magnification TEM pictures of SWCNT-glycol with oligonucleotide sequence 1, and complementary oligonucleotide 2 (ratio CNT/DNA of 1:10) The picture on the left is lower magnification than the one on the right.

The magnification pictures, at 63,000X and 125,000X show a much more relaxed aggregate form with slightly higher density on the center. The analysis of the picture

demonstrates that the most ideal molecular ratios for aggregate formation are 1:1:1 and 1:10:10 CNT/Oligo1/Complementary Oligo 2. Also, this shows these experiments demonstrated that the system could be used for gene detection at the nanomolar ratio, since in my experiments I was able to detect hybridization of 2.8 ug of the interest gene in 1.2 ml isopropanol/water solution.

CHAPTER 4

4.1 Conclusions

Spectroscopic evidence of f-MWCNTs and f-SWCNTs confirmed surface functionalization at different degrees; SWCNT-COOH/44.7%, SWCNT-Glycol/27.8%, and MWCNT-EDA/12%. This placed SWCNT-Glycol as maintaining a better sp2 nanotube framework than SWCNT-COOH, and based on the solubility properties of MWCNT-EDA revealed that 12% is too little for proper dispersion. The sample SWCNT-Glycol was chosen for its superior solubility properties and stability balance. The greatest evidence for this was that HNMR was collected, since it was the only sample that allowed shimming.

Although to different extents all f-CNT samples proved through UV-VIS to be soluble. Solubility experiments, spectroscopy, and microscopy confirm that DNA improves the dispersibility of the carbon nanotube samples giving much more significance to the findings of aggregates on this thesis. Raman spectroscopy also revealed through a shift in the I_D/I_G ratios that DNA interacted with the sp2 sites in the carbon nanotube; most likely through pi-pi stacking with DNA bases. Experiments also showed that carbon nanotubes have a high DNA loading capacity, in the case of the DNA/CNT Raman spectrum for SWCNT-Glycol, it makes one of the RBM to almost disappear.

One can conclude from this work that, based on all the evidence shown in this work, the dispersion properties of SWCNT-Glycol without DNA and SWCNT-Glycol/Oligo1 its strong enough evidence that sequence selective aggregation is occurring.

REFERENCES

1. S. Iijima, et al., Nature 354,6348 (1991) 56-8
2. J.W.G. Wildöer, L.C. Venema, A.G. Rinzler, R.E. Smalley, C. Dekker, Nature 59 (1998) 391
3. W. Clauss, D.J. Bergeron, M. Freitag, C.L. Kane, E.J .Mele, A.T. Johnson, Europhys. Lett. 47 (1999) 601
4. D. Tománek, S. Louie, H. Mamin, S. Abraham, R. Thomson, E. Ganz, and J. Clarke, Phys. Rev. B35 (1987) 7790
5. C.L. Kane, E.J. Mele, Phys. Rev. B59 (1999) R12759
6. R.C. Weast. (1988). Handbook of Chemistry and Physics, 69th Edition. Location: CRC Press
7. A. Arrais, E. Boccaleri, E.D. Fuller, Carbon Nanostructures 12 (2004) 789–809
8. N. Nakayama, et al, J. AmChemSoc 129,9 (2007) 2448–9.
9. J. Chattopadhyay, F. Cortez, et al. ChemMater18,25 (2006) 5864–8
10. B. Zhao, H Hu, A.P Yu, D. Perea, et al. JAmChemSoc 127,22 (2005) 8197–203
11. L. Lacerda, G. Pastorin, W. Wu, M. Prato, Adv. Funct. Mater. 16,14 (2006) 1839–46
12. K. Imasaka, J. Suehiro, Y. Kanatake, Nanotechnology 17,14, (2006) 3421–7
13. J.B. Kim, T. Premkumar, K. Lee, K.E. Geckeler, Macromol Rapid. Commun 28,3 (2007) 276–80
14. M.C. Paiva, B. Zhou, et al.,Carbon42,14 (2004) 2849–54
15. Y. Lin, A.M. Rao, B. Sadanadan, Et al., J. Phys. Chem. B2002 (2002) 1294–8
16. T. Zhang, M. Xu, L. He, K. Xi, Et al., Carbon 46 (2008) 1782-1791
17. J.A Olivier, S. Schueller, et al., Sensors and actuators A72 (1999) 125-139
18. R.L.C Thiago, W. Paixao, et al. Sensors and actuators B 87 (2002) 41-46

19. T. J. Bandosz, Et al. (2006) Activated carbon surfaces in environmental remediation. Location: Academic Press.
20. N. Yusuf, et al. J Mater Sci 44 (2009) 2774-2779
21. K.V. Sandee, D. Zheng, G. Pastorin, K. Al-Rubeaan, et al., Carbon 49 (2011) 4077-4097
22. H.J Dai, A. Javey, E. Pop, D. Mann, W. Kim, Y. Lu, Nano Brief Reports and Reviews 1 (2006) 1–4
23. A. Kis, A. Zettl, et al. Phil. Trans. R. Soc. A 366 (2008) 1591–1611
24. P. Kim, L. Shi, A. Majumdar, P.L. McEuen, Phys. Rev. Lett. 87 (2001) 215502
25. P. Chakravarty, R. Marches, N.S. Zimmerman, A.D. Swafford, et al. Proc. Natl. Acad. Sci. 105,25: (2008) 697–702
26. N.W Kam, M. O'Connell, J.A. Wisdom, H Dai. Proc. Natl. Acad. Sci. 102,33 (2005) 11600–5.
27. A. De La Zerda, C. Zavaleta, S. Keren, S. Vaithilingam, S. Bodapati, Z. Liu, et al. Nature Nanotechnology 3 (2008) 556-562
28. T. N. Narasimhan, et al. Physics Today 62(2009) 48-53
29. E. L. Cussler, et al. Diffusion: Mass Transfer in Fluid Systems. (2009)Cambridge UniversityPress,.
30. N. Coleman, et al. Carbon 44 (2006) 1624–1652
31. H. Zhidong, et al. Progress in Polymer Science 36 (2011) 914–944
32. A. Al-Rub, K. Rashid, et al. Construction and Building Materials 35 (2012) 647–655
33. K. Waqas, et al. Diamond & Related Materials 19 (2010) 1405–1410
34. P. Hui, et al. Physics Letters A 331 (2004) 231–237
35. L. Liyue, Y. Yingge, Z. Yafei. Physica E 24 (2004) 343–348
36. W. Merchan-Merchan, et al. Progress in Energy and Combustion Science 36 (2010) 696-727

37. M.S. Dresselhaus, G.Dresselhaus, Et al. Acc.Chem.Res., 35 (2002) 1070

38. M.S. Dresselhaus, G. Dresselhaus, Et al. PhysicsReports, 47 (2005) 409

39. R. Lee, Et al. Science, 273(1996) 483

40. R.B. Little. Et al. J. Cluster Sci. 14 (2003)135

41. A. Moisala, Et al. J Phys. Condens. Matter, 15 (2003) s3011

42. C. Depuis. Et al. Prog. Mater. Sc. 50 (2005) 929

43. H.Dai, et al. Acc.Chem.Res. 35 (2002)1035

44. R. Andreas, et al. Journal of Cleaner Production 16 (2008) 927-937

45. A.G Osorio, et al. App. surf. Sci. 25 (2008) 2485-2489

46. S. Toita, et al. Diamond and Related Materials 17 (2008) 1389–1393

47. U.J Kim, et al. Physical review letters 95 (2005) 157402

48. Blasej Scheibe, et al. Material characterization 61 (2010) 185-191

49. Arnold J. Gordon and Richard A. Ford. (1972). *The chemist's companion*. Wiley-Interscience publication

50. Suriani, A.B., et al. Material Letters 63 (2009) 2704-2706

51. F. Chammsedine, et al. Journal of Fluorine Chemistry 132 (2011) 1072-1078

52. Arepalli, Sivaram, et al. Carbon 42 (2004) 1783-1791

53. Yan-Yan, Lu, et al. Physica E (2010) 510-514

54. Strong L., Karla, et al. Carbon 41 (2003) 1477-1488

55. Madaleno, Liliana, et al. Composite s Science and Technology (2012) 377-381

56. Lebeckin, Frank, et al. Carbon 40 (2002) 417-423

57. Cheung et al. Advanced Drug Delivery Reviews 62 (2010) 633-649

CURRICULUM VITA

Hugo Alarcon Valenzuela was born in Distrito Federal, Mexico. The first son of Delia Valenzuela Gonzalez and Hugo Alarcon Quiroz, he graduated from CBTIS 128 High School, Ciudad Juarez, Chihuahua, in the spring of 2002 and entered the University of Texas at El Paso in the fall. While pursuing a bachelor's degree in Microbiology, he worked in the Peer-Led Team Learning program in the Chemistry department in UTEP, from the spring of 2003 to the fall of 2005. In the three years he served as a facilitator for chemistry in laboratory practices as well as theory, he also presented his work in education conferences. He later was admitted to work as a laboratory assistant with Dr. Juan C. Noveron in the spring of 2006. Place that allowed him to explore research in chemical engineering for medical and environmental applications. He then served as a guest presenter in scientific conferences held in West Palm Beach, Kansas City, Salt Lake City, and Washington D.C. In the fall of 2008, He was accepted to the Masters in Chemistry program in the University of Texas at El Paso.

Permanent Address: 8541 Bosque de Benjui
Ciudad Juarez, Chihuahua 32539
or
hvalarcon@miners.utep.edu